JOURNAL OF PETROLOGY | VOLUME 43 | NUMBER 8 | PAGES 1435–1467 | 2002

Petrogenesis of the Back-arc East Scotia Ridge, South Atlantic Ocean

S. FRETZDORFF[1]*, R. A. LIVERMORE[2], C. W. DEVEY[3], P. T. LEAT[2] AND P. STOFFERS[1]

[1]INSTITUTE OF GEOSCIENCES, UNIVERSITY OF KIEL, OLSHAUSENSTRASSE 40, 24118 KIEL, GERMANY

[2]BRITISH ANTARCTIC SURVEY, HIGH CROSS, MADINGLEY ROAD, CAMBRIDGE CB3 0ET, UK

[3]FACHBEREICH 5—GEOWISSENSCHAFTEN, UNIVERSITY OF BREMEN, POSTFACH 330 440, 28334 BREMEN, GERMANY

RECEIVED JANUARY 3, 2001; REVISED TYPESCRIPT ACCEPTED JANUARY 22, 2002

The East Scotia Ridge is an active back-arc spreading centre located to the west of the South Sandwich island arc in the South Atlantic Ocean, consisting of nine main segments, E1 (north) to E9 (south). Major and trace element and Sr–Nd–Pb isotope compositions are presented, together with water contents, for lavas sampled along the active ridge axis. Magmatism along the East Scotia Ridge is chemically heterogeneous, but there is a common mid-ocean ridge basalt (MORB)-type source component for all the magmas. An almost unmodified MORB-source mantle appears to underlie the central part of the back-arc. Subduction components are found at the northern and southern ends of the ridge, and there is a marked sediment melt input of up to 2% in segment E4. Enriched (plume) mantle is present beneath segment E2 at the northern end of the ridge, suggesting that plume mantle is flowing westward around the edges of the subducting slab. The southern part of segment E8 is unique in that its magma source is similar to sub-arc depleted mantle.

KEY WORDS: *geochemistry; petrogenesis; volcanism; back-arc; subduction*

INTRODUCTION

Fractional melting of mantle peridotite is the primary source of back-arc magmas and it has been postulated that the major source component should be similar to that of mid-ocean ridge basalt (MORB, e.g. Hawkins, 1976; Saunders & Tarney, 1979). However, most back-arc basin basalts have geochemical characteristics that show that subduction processes are also involved in their petrogenesis, e.g. basalts erupted in the Mariana Trough and the Lau Basin (e.g. Hawkins, 1976; Hawkins & Melchior, 1985; Volpe *et al.*, 1987; Stern *et al.*, 1990; Gribble *et al.*, 1998; Turner & Hawkesworth, 1998; Peate *et al.*, 2001). These characteristics provide evidence for prior depletion of the mantle source and enrichment in H_2O and elements such as Ba, Th, U and Pb, thought to be transported into the mantle wedge from the subducting slab via sediment melts or aqueous fluids (Stern *et al.*, 1990; Saunders *et al.*, 1991; Woodhead *et al.*, 1993; Stolper & Newman, 1994; Pearce *et al.*, 1995; Gribble *et al.*, 1998). Back-arc basins can therefore be used to model the transport of slab components into the mantle wedge over much wider areas in subduction zone environments than can be achieved by studying volcanic arcs alone, and can be used to test models of mantle wedge convection. Furthermore, the transitional character of back-arc basalts from MORB to arc-like provides critical evidence of the relative roles of decompression vs volatile fluxed melting of mantle (Gribble *et al.*, 1998).

The East Scotia Ridge, an active back-arc spreading centre behind the South Sandwich island arc in the South Atlantic Ocean (Fig. 1), is an interesting place to study subduction-related processes for several reasons: (1) its simple tectonic setting as part of an intra-oceanic arc, without the influence of continental crust; (2) its close proximity to the active island arc, suggesting the possibility of a strong subduction influence on the back-arc mantle source (Livermore *et al.*, 1997); (3) the well-defined chemical signature of the associated island arc (Pearce *et al.*, 1995) and of the sediments subducting at the South Sandwich trench (Barreiro, 1983; Ben Othman *et al.*,

*Corresponding author. Telephone: ++49 431 880 2085. Fax: ++49 431 880 4376. E-mail: sf@gpi.uni-kiel.de

1989; Plank & Langmuir, 1998). Recent campaigns by the British Antarctic Survey (Livermore *et al.*, 1999) and the University of Kiel now provide sampling of the neo-volcanic zone within each segment of the East Scotia Ridge. In this paper, we present major and trace element compositions together with Sr–Nd–Pb isotope data for basalt samples dredged from the ridge axis, to identify petrogenetic processes controlling geochemical variations and to identify the components contributing to the magma source of the East Scotia Ridge lavas.

TECTONIC SETTING

The East Scotia Ridge is situated some 250–300 km to the west of the South Sandwich trench (Fig. 1). It was mapped for the first time in 1995 using the HAWAII-MR1 swath sonar (Livermore *et al.*, 1995) and shown to consist of nine segments, separated by non-transform offsets. Spreading rates of 60–70 km/Myr place it in the intermediate range of spreading centres, transitional between 'fast' (axial high) and 'slow' (median valley) morphologies. Six segments, E3–E8, are characterized by faulted median valleys similar to those observed at the Mid-Atlantic Ridge, whereas segments E2 and E9 both display axial volcanic ridges (Fig. 2), and are propagating into the back-arc region (Livermore *et al.*, 1997; Bruguier & Livermore, 2001). Segment E1 extends northward into the South Sandwich trench in the form of a trough with water depths of up to 5500 m. Side-scan images of this segment show it to be surrounded by a much more chaotic backscatter pattern compared with the rest of the East Scotia Ridge, indicating recent establishment of E1 and/or a more disordered mode of extension (Livermore *et al.*, 1997). There is a distinct along-axis trend in axial depth, from maxima of >4000 m in segments E5 and E6, to minima of ~2600 m in E2 and E9. These characteristics have provided support for models involving the shallow inflow of Atlantic mantle around the ends of the subducting slab (Livermore *et al.*, 1997).

The South American plate is subducting beneath the Sandwich plate at a rate of 70–85 km/Myr (Pelayo & Wiens, 1989). Earthquake data indicate that the subducting plate dips at 45–55° to the west, probably steepening slightly in the southern part of the subduction zone (Brett, 1977). The age of the subducting plate is 28–35 Ma below the southern part of the arc, and 50–60 Ma below the northern part of the arc (Sclater *et al.*, 1976; Barker & Lawver, 1988). The sedimentary cover on the subducting plate consists of some 200 m of siliceous sediments in the south, and some 400 m of calcareous and siliceous sediments in the north (Barker, 1995). More than 95% of this sediment input to the trench is subducted, and there is no significant sediment accretion at the trench (Vanneste & Larter, 2002).

The South Sandwich arc consists of 11 main islands forming a distinctly curved island arc, 500 km in length. Most of the islands have abundant evidence of recent volcanic activity, and all are entirely volcanic in origin. The volcanoes belong to the tholeiitic and (relatively rare) calc-alkaline series, and the arc is regarded as a classic example of the primitive stages of island arc development (Baker, 1968, 1990; Pearce *et al.*, 1995). All the arc magmas are depleted in high field strength elements (HFSE) such as Ti, Zr, Hf, Nb and Ta, and heavy rare earth elements (HREE), relative to normal MORB, and are therefore thought to be derived from mantle wedge material that had experienced melt extraction before the magma generation events (Hawkesworth *et al.*, 1977; Pearce *et al.*, 1995). All the magmas are enriched (relative to MORB) in highly incompatible fluid-mobile trace elements, such as Pb, U, Ba and Rb, derived from the subducting plate. Pearce *et al.* (1995) suggested that variations in incompatible trace element abundances were a result of dynamic melting processes within the sub-arc mantle and that the Nd and Sr isotope covariations of the island arc sample suite indicate the involvement of a subduction component derived from the subducted sediment and altered oceanic crust. We argue below that the sediment-derived component has locally influenced the back-arc magmatism.

Previous geochemical studies

Previous investigations of lavas from the East Scotia Ridge were confined to eight dredge sites (D20–D24, D56, D57, D60) sampled by R.R.S. *Shackleton* in 1974 and 1981, as well as volcanic rocks from the axis and the lateral flanks of segment E2 and the northern part of E3, sampled by R.R.S. *James Clark Ross* in 1996 (Fig. 2). Dredge sites were located on the northern tip of segment E3 (D20), east of the southern tip of E2 (D21), west of segment E5 (D22), close to the northern tip of segment E9 (D24), in the centre of segment E9 (D23), and east of the northernmost segment E1 (D56). Apart from the recently sampled segment E2 and the northern part of E3, only the dredge stations D20 and D23 are located in the neo-volcanic axis of the East Scotia Ridge. The petrographic characteristics, major and trace element geochemistry, volatile content, and Sr, Nd, Pb, O and C isotope compositions of lavas dredged at the four locations D20 and D22–24 have been reported in earlier studies (Hawkesworth *et al.*, 1977; Tarney *et al.*, 1977; Saunders & Tarney, 1979; Muenow *et al.*, 1980; Cohen & O'Nions, 1982*a*; Saunders *et al.*, 1982; Mattey *et al.*, 1984; Newman & Stolper, 1996; Eiler *et al.*, 2000). These studies showed that the lavas have an intermediate

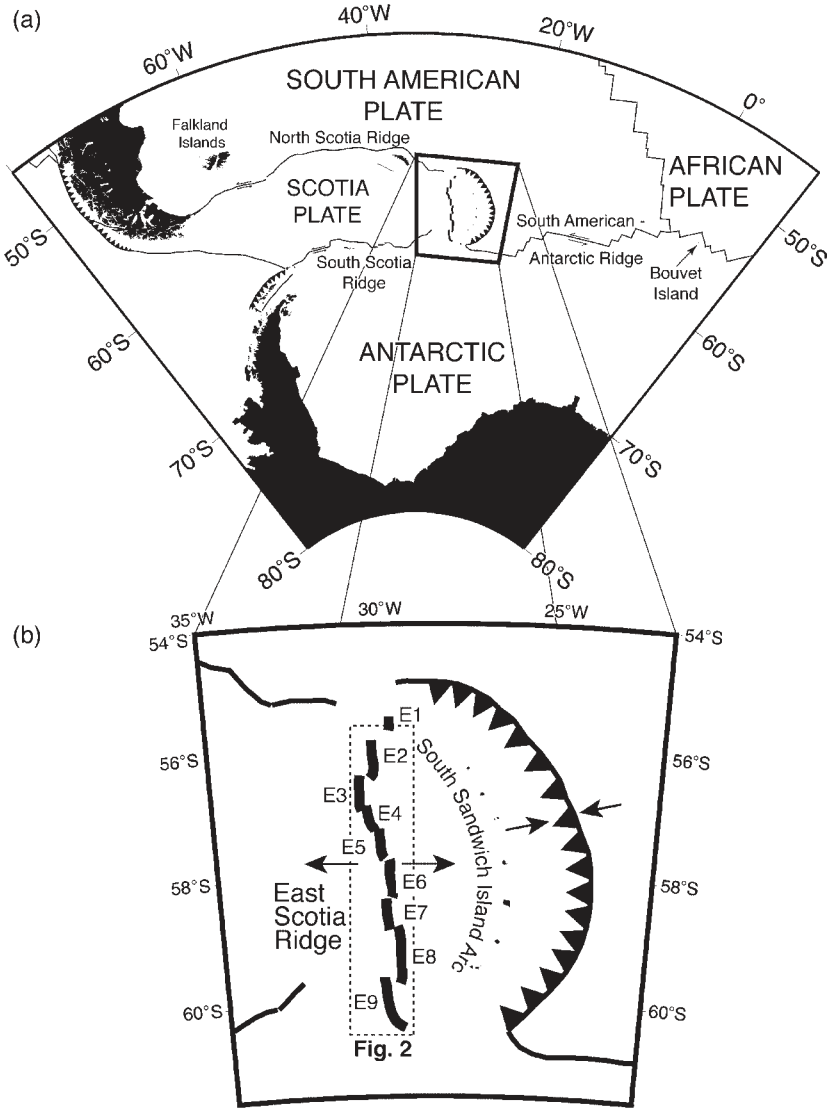

Fig. 1. (a) Tectonic setting of the East Scotia Ridge within the Scotia Sea area. (b) Sketch map of the South Sandwich subduction zone with the location of the East Scotia Ridge segments (E1–E9) and South Sandwich Islands (after Leat *et al.*, 2000). The arrows mark the spreading direction along the East Scotia Ridge and the relative movement of the subducting plate.

geochemical composition between MORB and island-arc tholeiite, leading to the suggestion that fluids and/or sediments derived from the subducting slab influence the mantle source of the East Scotia Ridge basalts (e.g. Saunders & Tarney, 1979; Tarney *et al.*, 1981; Saunders *et al.*, 1982). More recently, Pearce *et al.* (2001) reanalysed a suite of samples from dredge sites on segments E3 and E9. They showed that the back-arc lavas have Pb and Nd isotope characteristics of South Atlantic, rather than Pacific mantle. This implies that any outflow of Pacific MORB through the Drake Passage as suggested by Alvarez (1982) does not extend as far as the East Scotia Ridge.

Most of the back-arc lavas have lower $^{206}Pb/^{204}Pb$ ratios than those of the South American–Antarctic Ridge (Pearce *et al.*, 2001). The characteristic geochemical signature of the South American–Antarctic Ridge basalts is interpreted to be the result of a westward asthenospheric flow of enriched mantle from the Bouvet plume along the ridge axis (e.g. Le Roex *et al.*, 1985). Pearce *et al.* (2001) suggested that this Bouvet plume component is also present in the East Scotia Ridge mantle source as a result of asthenospheric inflow into the back-arc region from the north and south. Leat *et al.* (2000) carried out a detailed geochemical study of the E2 segment. Their results support the interpretation of Pearce *et al* (2001)

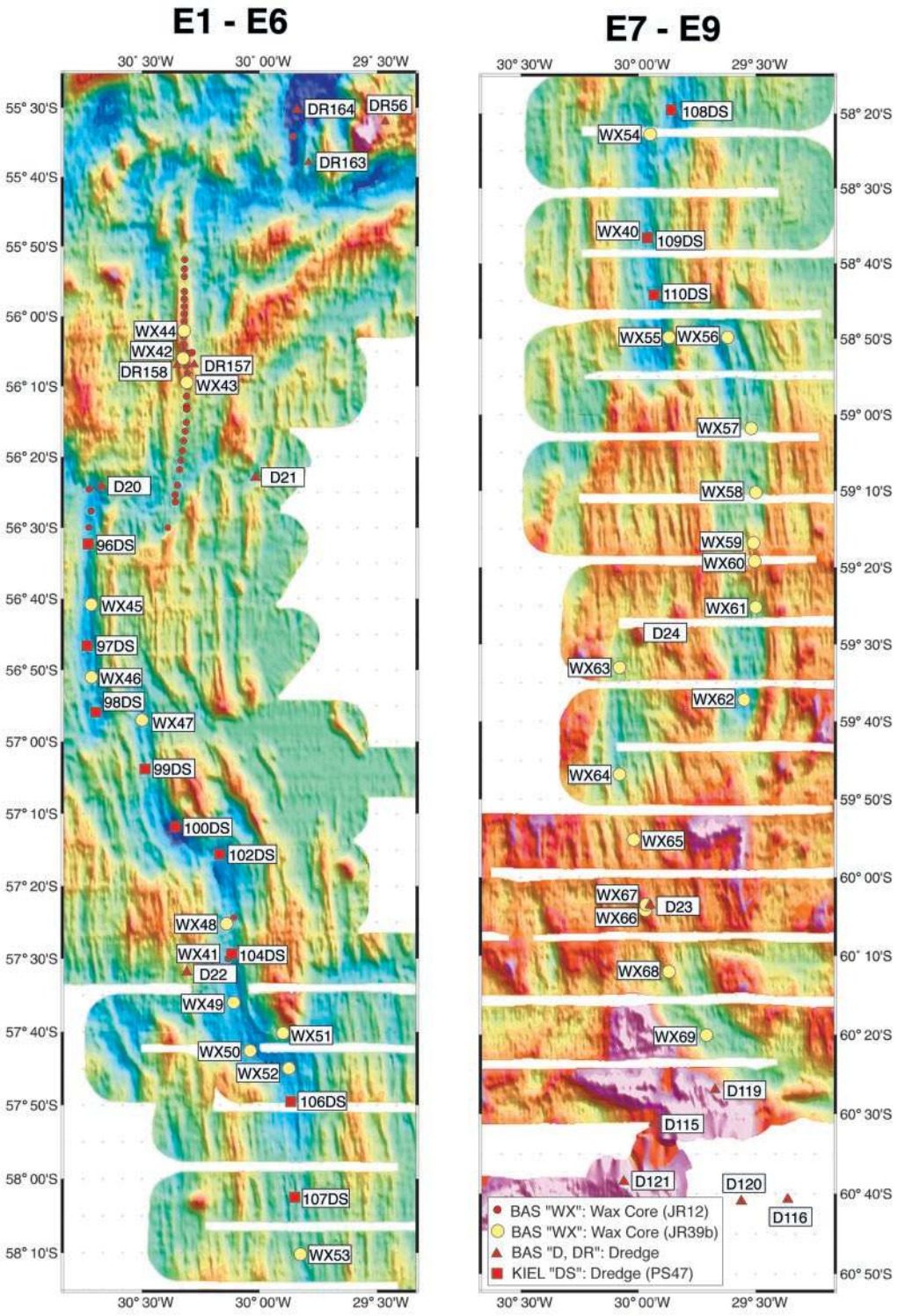

Fig. 2. HAWAII-MR1 bathymetry of the East Scotia Ridge, showing sample locations occupied during British Antarctic Survey (BAS) cruises JR09 (dredged samples: red triangles), JR12 (wax core samples: red circles; dredged samples: red triangles), JR39b (wax core samples: yellow circles) and the German *Polarstern* cruise PS47 (dredged samples: red squares).

that material from the Bouvet mantle plume is migrating westwards into the back-arc, and showed that lavas from the flanks of segment E2 have a higher plume influence than axial lavas. Furthermore, they demonstrated the contribution of a slab-derived component to most E2 lavas.

Sampling

Sampling stations on the active part of the back-arc spreading ridge were selected on the basis of detailed side-scan sonar and bathymetric data (Livermore *et al.*, 1995; Fig. 2). In 1997–1998, sampling of segments E3–E7 was carried out using a drum-shaped dredge during R.V. *Polarstern* cruise PS47 (ANT XV/II), with general dredge direction along the spreading axis. Fresh volcanic material, e.g. pillow lavas, sheet flows and lava tubes, most of which preserved fresh glassy margins, were recovered during the 10 dredge deployments during cruise PS47 (Fig. 2). During R.R.S. *James Clark Ross* cruise JR39b in 1999, fresh volcanic glass fragments were obtained at 28 sites from segments E2 to E9 using a wax corer (Livermore *et al.*, 1999). These fresh volcanic samples, when combined with previous high-density sampling of segment E2 (Leat *et al.*, 2000) during cruise JR12, provide complete coverage of the East Scotia Ridge neo-volcanic zone (Fig. 2, coordinates listed in Table 1).

ANALYTICAL METHODS

Macroscopic criteria (vesicularity; size, abundance and variety of minerals) were used to select different rock types from each dredge haul, from which glassy pillow rims were separated under a binocular microscope and washed several times in ultra-pure water. Glass fragments in wax cups from the wax corer were removed from the wax with tweezers. The fragments were then placed into a beaker with water in a microwave oven for 2 min to melt the wax. The beaker was cooled and the wax removed. The sample was then washed several times in ultra-pure water.

Analyses of minerals were made at the University of Kiel (Institut für Geowissenschaften) with a Cameca CAMEBAX electron microprobe running at a beam current of 12·5 nA and acceleration voltage of 14–15 kV. Usually, the beam width was about 1–2 μm, and was defocused for plagioclase analyses. Synthetic and natural standards were used to calibrate the microprobe. Repeat measurements show that the relative standard deviations are smaller than ±0·5%, indicating a good reproducibility for all major elements. The major element concentrations of the volcanic glass samples were determined with a Cameca SX50 electron microprobe at GEOMAR (Kiel) (Table 1). A beam current of 10 nA with an accelerating voltage of 15kV was used. The beam was defocused to 5 μm to minimize Na loss during measurements. Glass analyses reported are the averages of more than five individual spot analyses (Table 1) with relative standard deviations smaller than ±0·5%. International glass standards (JDF-D2, CFA47 2) were measured after every 20 analyses to check precision, which is better than ±0·7%.

H_2O analyses were obtained by Fourier transform infrared (FTIR) spectroscopy at the University of Kiel using the methods and calibration described by Stolper (1982). Double-polished glass thin sections, 100–250 μm thick, were analysed with a Bruker IFS 66v/S FTIR spectrometer equipped with a Bruker A 590 Infrared Microscope with a mercury–cadmium–telluride detector. Optically clear areas of known thickness (±5 μm) were measured with aperture size of 120 μm diameter with 256 scans per spot. Concentrations were calculated using the Beer–Lambert law (e.g. Stolper, 1982) with assumed densities of 2·7 g/cm^3. Replicate analyses of different glass fragments from the same specimen were typically reproducible to ±10%. Comparison of the H_2O concentrations of two basalt glasses (EN112 4D-10; P1505-1) analysed by FTIR spectroscopy at the University of Tulsa (USA) (Michael, 1995) with the FTIR analyses at University of Kiel show reproducibility better than ±5%.

Trace element concentrations were determined by inductively coupled plasma mass spectrometry (ICP-MS) with a VG PlasmaQuad PQ1 system at the University of Kiel, using preparation and measurement methods described by Garbe-Schönberg (1993). Analytical accuracy and reproducibility are estimated from measurements of international rock standards BHVO-1 and BIR, and duplicate analyses of samples (Table 1). The accuracy of the standards is within ±10% of the suggested working values (Jenner *et al.*, 1990; Govindaraju, 1994), but generally better than ±5% for rare earth elements (REE). Duplicate analyses show reproducibility to be better than 3%, except for the transition metals (e.g. Cr, Ni, Cu, Zn, Ga) and elements with very low concentrations (e.g. Cs), which show deviations of up to 20% (Table 1).

Sr, Nd and Pb isotope ratios of volcanic glasses were measured on a MAT262-RPQ2+ thermal ionization mass spectrometer at GEOMAR in static mode. Glass chips were leached for 1 h in 6N HCl before sample dissolution, and analytical procedures followed those described by Hoernle & Tilton (1991). $^{87}Sr/^{86}Sr$ ratios were normalized to $^{86}Sr/^{88}Sr = 0{\cdot}1194$ within-run and $^{143}Nd/^{144}Nd$ ratios to $^{146}Nd/^{144}Nd = 0{\cdot}7219$. The long-term reproducibility of NBS 987 in this laboratory is $^{87}Sr/^{86}Sr = 0{\cdot}710254 \pm 17$ ($n = 83$) and of La Jolla $^{143}Nd/^{144}Nd = 0{\cdot}511845 \pm 11$ ($n = 123$). The in-house SPEX monitor, calibrated against La Jolla with $^{143}Nd/^{144}Nd = 0{\cdot}511706 \pm 12$ ($n = 9$), yielded $^{143}Nd/^{144}Nd = 0{\cdot}511705$

Table 1: Location, water depth and geochemical analyses of the East Scotia Ridge volcanic glasses

Segment:	E2	E2	E2	E3	E3	E3	E3	E3	E3	E3	E3
Sample:	wx44	wx42	wx43	96DS-1	96DS-2	96DS-3	96DS-4	wx45	97DS-1	97DS-2	97DS-4
Lat. (S):	56°02·01′	56°06·03′	56°09·40′	56°32·3′	56°32·3′	56°32·3′	56°32·3′	56°40·00′	56°46·6′	56°46·6′	56°46·6′
Long. (W):	30°19·51′	30°19·51′	30°18·51′	30°43·7′	30°43·7′	30°43·7′	30°43·7′	30°43·00′	30°44·0′	30°44·0′	30°44·0′
Depth (m):	2840	2758	2885	3880	3880	3880	3880	3730	3949	3949	3949
Major elements by electron microprobe (wt %); H_2O by FTIR (wt %)											
*n*ME/*n*H_2O	10	12/4	12/3	19/3	19	21/5	15	18/8	10	9/2	10
SiO_2	52·70	53·40	53·08	50·26	50·22	50·64	50·27	49·65	51·55	51·58	51·87
TiO_2	1·69	1·61	1·99	1·23	1·24	1·54	1·24	1·32	1·71	1·69	1·71
Al_2O_3	15·14	15·15	15·12	16·34	16·34	15·64	16·36	15·33	15·95	15·94	15·88
FeO	8·94	8·93	9·95	7·82	7·78	8·62	7·84	8·31	8·23	8·13	8·05
MnO	0·20	0·20	0·20	0·16	0·15	0·16	0·16	0·17	0·16	0·16	0·18
MgO	4·77	4·98	4·21	8·16	8·15	7·39	8·17	8·25	6·94	6·95	6·97
CaO	9·04	9·07	7·97	11·21	11·21	10·87	11·18	11·80	10·38	10·40	10·36
Na_2O	3·75	3·66	4·02	2·97	2·95	3·11	2·95	3·09	3·39	3·38	3·39
K_2O	0·49	0·52	0·47	0·13	0·12	0·16	0·12	0·11	0·21	0·21	0·23
P_2O_5	0·36	0·37	0·42	0·26	0·27	0·29	0·27	0·26	0·35	0·33	0·37
H_2O	n.d.	0·77	1·02	0·24	n.d.	0·43	n.d.	0·12	n.d.	0·45	n.d.
Total	97·08	98·67	98·45	98·79	98·85	98·42	98·57	98·41	98·88	99·24	99·01
mg-no.	52·83	53·92	47·04	68·64	68·72	64·25	68·62	67·58	63·89	64·20	64·50
Trace elements by ICP-MS (ppm)											
Sc	31·5	29·8	30·9	30·5		33·2		35·7	33·5		
Cr	70·4	54·3	10·8	302		247		324	213		
Co	28·3	26·3	28·1	36·3		35·8		36·3	35·0		
Ni	37·0	32·1	8·99	130		96·9		124	95·5		
Cu	46·9	49·6	36·3	52·7		48·5		59·4	45·1		
Zn	80·2	81·6	91·0	71·3		80·5		56·7	89·5		
Ga	17·4	17·4	18·7	14·5		16·0		14·7	16·7		
Rb	6·83	7·97	7·45	2·34		3·63		1·02	5·50		
Sr	234	244	211	129		130		104	148		
Y	27·5	27·4	33·2	22·0		29·5		24·4	33·2		
Zr	118	114	144	70·6		89·0		70·8	115		
Nb	8·53	7·79	9·72	2·45		3·44		1·58	3·93		
Cs	0·105	0·131	0·127	0·016		0·033		0·014	0·048		
Ba	107	114	117	20·2		30·9		12·3	38·3		
La	9·08	9·02	10·3	3·12		4·04		2·35	5·15		
Ce	20·7	20·7	24·3	9·26		11·9		7·40	15·4		
Pr	3·04	2·99	3·55	1·59		2·04		1·40	2·57		
Nd	13·9	13·8	16·3	8·17		10·5		7·89	13·0		
Sm	3·92	3·89	4·63	2·82		3·56		2·86	4·35		
Eu	1·36	1·34	1·59	1·05		1·25		1·07	1·48		
Gd	4·59	4·54	5·58	3·71		4·72		3·89	5·51		
Tb	0·798	0·796	0·958	0·665		0·850		0·693	0·966		
Dy	5·11	5·12	6·13	4·53		5·71		4·62	6·48		
Ho	1·09	1·08	1·30	0·925		1·18		0·986	1·34		
Er	3·05	3·06	3·69	2·59		3·31		2·93	3·81		
Tm	0·449	0·447	0·539	0·387		0·495		0·403	0·560		
Yb	2·97	3·00	3·55	2·59		3·30		2·63	3·71		
Lu	0·439	0·444	0·531	0·371		0·469		0·385	0·536		
Hf	3·01	2·99	3·66	2·27		2·90		2·17	3·61		
Ta	0·484	0·435	0·553	0·152		0·207		0·105	0·237		
Tl	0·032	0·037	0·034	n.d.		0·003		0·007	0·008		
Pb	1·17	1·49	1·29	0·448		0·492		0·376	0·682		
Th	0·977	0·989	1·05	0·177		0·259		0·111	0·315		
U	0·272	0·268	0·305	0·052		0·077		0·038	0·093		

Segment:	E3	E3	E3	E4	E4	E4	E4	E4	E5	E5	E5
Sample:	97DS-5	wx46	98DS-1	wx47	99DS-1	99DS-3	99DS-4	100DS-1	102DS-1b	wx48	104DS-1
Lat. (S):	56°46·6′	56°51·00′	56°55·9′	57°02·01′	57°03·8′	57°03·8′	57°03·8′	57°11·8′	57°15·6′	57°25·19′	57°29·3′
Long. (W):	30°44·0′	30°42·91′	30°41·8′	30°30·00′	30°29·2′	30°29·2′	30°29·2′	30°21·5′	30°10·2′	30°08·41′	30°07·1′
Depth (m):	3949	3790	3891	3681	3688	3688	3688	4568	4155	3683	3779
Major elements (wt %)											
*n*ME/*n*H_2O	13/3	16	14/5	18	10/3	15	14	25/6	9	21/6	18/2
SiO_2	51·72	50·92	52·15	50·88	54·19	53·30	53·20	51·55	52·55	49·83	51·72
TiO_2	1·70	1·69	1·40	1·48	1·27	1·16	1·16	1·46	1·49	1·33	1·69
Al_2O_3	15·93	15·46	16·04	16·26	16·80	17·24	17·32	15·63	15·62	15·30	15·44
FeO	8·07	8·73	7·57	7·88	6·47	6·46	6·42	7·94	8·26	8·26	8·30
MnO	0·17	0·19	0·17	0·18	0·15	0·14	0·14	0·16	0·17	0·18	0·18
MgO	7·02	6·63	6·83	6·35	5·85	5·94	5·97	7·42	6·10	8·13	7·02
CaO	10·35	10·48	10·82	10·82	9·40	9·39	9·39	10·68	9·81	11·60	10·46
Na_2O	3·37	3·20	2·81	3·02	2·66	2·63	2·63	3·06	3·24	3·29	3·37
K_2O	0·21	0·39	0·42	0·59	0·93	0·96	0·97	0·19	0·21	0·10	0·17
P_2O_5	0·34	0·34	0·30	0·34	0·32	0·32	0·32	0·26	0·26	0·26	0·30
H_2O	0·48	n.d.	1·63	n.d.	2·25	n.d.	n.d.	0·69	n.d.	0·18	0·63
Total	99·36	98·04	100·15	97·80	100·28	97·55	97·52	99·04	99·15	98·46	99·29
mg-no.	64·59	61·45	65·44	62·83	65·50	65·87	66·09	66·22	60·77	67·36	63·94
Trace elements (ppm)											
Sc		38·8	29·3	34·2	26·2		24·8	31·6	29·0	33·6	31·9
Cr		179	191	169	114		107	222	163	328	207
Co		33·7	31·5	29·6	26·2		26·1	34·8	32·4	38·4	34·2
Ni		80·8	78·9	80·2	86·2		78·7	92·5	75·1	99·0	82·5
Cu		42·1	43·1	53·9	35·4		32·9	44·2	49·7	64·7	48·8
Zn		67·8	80·2	70·0	63·3		61·3	76·9	132	68·9	87·8
Ga		16·8	15·5	16·5	16·3		16·4	15·7	16·9	15·8	16·2
Rb		7·51	10·2	11·7	25·9		26·3	3·56	4·17	0·697	2·50
Sr		179	177	237	298		312	145	139	145	143
Y		33·5	24·3	28·2	20·5		19·4	27·2	26·5	26·2	32·1
Zr		115	80·9	110	74·6		72·5	92·7	91·0	96·5	113
Nb		5·06	3·91	4·43	5·31		5·49	3·10	2·51	2·06	2·91
Cs		0·131	0·136	0·222	0·420		0·426	0·039	0·072	0·013	0·026
Ba		100	102	143	268		284	30·1	31·1	8·74	19·0
La		5·86	4·97	5·98	8·30		8·41	4·34	4·12	2·94	4·90
Ce		16·0	13·1	15·5	19·8		20·0	12·3	12·0	9·32	14·3
Pr		2·59	2·08	2·42	2·72		2·70	2·05	1·98	1·69	2·45
Nd		13·2	10·1	12·0	12·3		12·1	10·6	10·1	8·97	12·4
Sm		4·26	3·25	3·70	3·33		3·31	3·56	3·40	3·12	4·07
Eu		1·44	1·16	1·29	1·14		1·09	1·27	1·22	1·18	1·41
Gd		5·40	4·18	4·55	3·77		3·64	4·59	4·35	4·05	5·22
Tb		0·948	0·721	0·804	0·625		0·608	0·828	0·779	0·729	0·929
Dy		6·26	4·90	5·18	4·08		3·99	5·58	5·22	4·79	6·23
Ho		1·33	1·01	1·11	0·827		0·793	1·14	1·07	1·02	1·30
Er		3·98	2·83	3·14	2·33		2·24	3·25	3·07	2·85	3·60
Tm		0·548	0·420	0·464	0·353		0·340	0·478	0·454	0·416	0·535
Yb		3·60	2·81	3·03	2·39		2·30	3·17	3·00	2·74	3·61
Lu		0·532	0·408	0·450	0·351		0·345	0·470	0·445	0·401	0·520
Hf		3·32	2·63	2·92	2·42		2·43	2·92	2·79	2·53	3·55
Ta		0·325	0·252	0·288	0·351		0·357	0·197	0·164	0·150	0·194
Tl		0·033	0·026	0·054	0·079		0·078	0·004	0·007	0·011	0·005
Pb		0·865	0·820	1·12	2·06		2·11	0·627	0·886	0·469	n.d.
Th		0·540	0·506	0·653	1·38		1·46	0·269	0·290	0·109	0·228
U		0·156	0·137	0·186	0·341		0·349	0·083	0·092	0·048	0·083

Table 1: continued

Segment:	E5	E5	E5	E5	E6	E6	E6	E6	E6	E6	E6
Sample:	104DS-3	wx41	wx49	wx50	wx51	wx52	106DS-1	106DS-2	106DS-3	106DS-4	107DS-1
Lat. (S):	57°29·3′	57°29·3′	57°36·00′	57°42·59′	57°40·21′	57°45·00′	57°49·5′	57°49·5′	57°49·5′	57°49·5′	58°02·5′
Long. (W):	30°07·1′	30°07·99′	30°06·62′	30°02·36′	29°53·96′	29°52·50′	29°52·0′	29°52·0′	29°52·0′	29°52·0′	29°51·0′
Depth (m):	3779	3912	3995	4151	3264	4090	3973	3973	3973	3973	3531
Major elements (wt %)											
*n*ME/*n*H_2O	17/5	18	18/6	17/6	17/4	4	12/3	14/6	14/6	11/4	34/12
SiO_2	51·96	51·12	50·30	50·35	50·95	51·89	49·79	50·23	50·20	49·69	49·32
TiO_2	1·77	1·60	1·39	1·52	1·73	1·78	1·66	1·66	1·71	1·68	1·44
Al_2O_3	15·20	16·31	16·27	15·17	15·07	14·77	14·84	15·55	15·54	15·40	16·34
FeO	8·44	8·75	8·12	9·10	9·41	10·24	9·18	9·20	9·03	9·27	8·05
MnO	0·20	0·20	0·18	0·20	0·20	0·23	0·21	0·18	0·18	0·19	0·15
MgO	6·77	6·56	8·16	7·72	7·47	7·12	7·82	7·72	7·73	7·66	7·93
CaO	10·41	10·03	11·38	11·27	11·14	11·86	10·94	10·98	10·97	10·90	11·32
Na_2O	3·36	3·75	3·43	3·16	3·18	3·15	2·91	2·96	2·97	2·96	3·47
K_2O	0·18	0·20	0·13	0·13	0·13	0·07	0·10	0·10	0·09	0·10	0·14
P_2O_5	0·30	0·34	0·30	0·29	0·32	0·34	0·26	0·30	0·29	0·29	0·27
H_2O	0·64	n.d.	0·23	0·29	0·36	n.d.	0·20	0·19	0·17	0·16	0·25
Total	99·22	98·87	99·89	99·20	99·96	101·45	97·90	99·06	98·86	98·29	98·68
mg-no.	62·74	61·14	67·82	64·02	62·49	59·32	64·13	63·76	64·24	63·44	67·38
Trace elements (ppm)											
Sc	31·2	33·7	30·7	36·9	34·5		29·9	32·1			29·8
Cr	205	205	250	292	267		227	231			251
Co	34·3	33·4	36·7	38·2	37·8		37·8	38·7			38·5
Ni	82·7	89·1	119	116	119		99·8	98·5			91·6
Cu	46·2	50·5	58·3	58·4	60·5		47·1	47·1			60·6
Zn	78·9	80·6	64·6	78·5	83·4		113	83·5			69·9
Ga	16·1	17·2	15·0	16·3	16·5		15·8	16·1			15·4
Rb	2·21	2·46	0·859	1·06	2·34		1·28	1·37			1·37
Sr	141	155	179	141	119		99·2	104			179
Y	30·3	33·8	24·2	29·5	34·1		31·2	32·1			24·4
Zr	112	134	107	108	118		92·5	93·6			90·7
Nb	2·99	3·20	2·60	2·43	2·28		1·94	1·94			2·45
Cs	0·018	0·057	0·011	0·023	0·052		0·002	0·003			0·006
Ba	18·0	25·1	11·7	15·4	26·1		10·9	10·3			12·1
La	4·67	4·83	3·90	3·61	3·81		3·23	3·22			3·88
Ce	14·5	14·2	11·8	11·0	11·7		10·5	10·8			11·6
Pr	2·43	2·43	1·97	1·93	2·10		1·94	1·98			1·98
Nd	12·3	12·3	10·0	10·0	11·1		10·4	10·7			10·0
Sm	4·00	4·02	3·21	3·46	3·90		3·76	3·86			3·38
Eu	1·40	1·44	1·17	1·21	1·34		1·30	1·34			1·23
Gd	5·20	5·22	4·03	4·52	5·10		5·04	5·14			4·20
Tb	0·913	0·934	0·717	0·826	0·939		0·921	0·948			0·746
Dy	6·11	6·11	4·65	5·51	6·20		6·28	6·47			4·98
Ho	1·26	1·31	0·984	1·19	1·34		1·30	1·33			1·00
Er	3·54	3·69	2·79	3·35	3·79		3·66	3·77			2·80
Tm	0·538	0·546	0·404	0·491	0·558		0·543	0·559			0·414
Yb	3·51	3·59	2·60	3·25	3·64		3·65	3·77			2·75
Lu	0·511	0·530	0·380	0·482	0·540		0·529	0·562			0·403
Hf	3·48	3·30	2·58	2·78	3·20		3·14	3·21			2·75
Ta	0·198	0·216	0·189	0·170	0·153		0·128	0·128			0·157
Tl	0·006	0·022	0·011	0·012	0·039		n.d.	n.d.			n.d.
Pb	n.d.	0·828	0·553	0·526	1·57		0·463	0·445			0·565
Th	0·224	0·265	0·148	0·147	0·261		0·134	0·119			0·152
U	0·086	0·104	0·061	0·062	0·070		0·052	0·039			0·056

Segment:	E6	E6	E6	E6	E7	E7	E7	E7	E7	E7	E7
Sample:	107DS-3	107DS-4	wx53	108DS-1	wx54b	109DS-1	109DS-2	109DS-3	109DS-4	109DS-5	109DS-6
Lat. (S):	58°02·5′	58°02·5′	58°10·21′	58°19·5′	58°22·97′	58°36·6′	58°36·6′	58°36·6′	58°36·6′	58°36·6′	58°36·6′
Long. (W):	29°51·0′	29°51·0′	29°49·52′	29°51·6′	29°57·23′	29°57·7′	29°57·7′	29°57·7′	29°57·7′	29°57·7′	29°57·7′
Depth (m):	3531	3531	3550	3999	3570	3636	3636	3636	3636	3636	3636
Major elements (wt %)											
*n*ME/*n*H_2O	22/4	20/3	6	25/4	22/2	22	16/4	17/4	23	23	18
SiO_2	50·31	49·70	50·12	50·63	51·19	50·38	50·49	51·15	50·67	50·24	49·97
TiO_2	1·45	1·45	1·11	1·68	2·11	1·47	1·50	1·61	1·49	1·51	1·49
Al_2O_3	15·16	16·31	16·89	15·24	14·46	15·58	15·61	15·21	15·61	15·44	15·55
FeO	8·75	8·07	7·23	8·74	10·51	8·75	8·71	9·48	8·68	8·74	8·71
MnO	0·19	0·17	0·15	0·18	0·21	0·18	0·16	0·19	0·18	0·19	0·17
MgO	8·10	7·86	8·56	7·68	7·25	7·75	7·56	7·65	7·81	7·60	7·72
CaO	11·95	11·29	11·20	11·14	10·63	11·24	11·28	11·35	11·25	11·24	11·25
Na_2O	2·42	3·46	2·78	2·95	3·21	3·49	3·51	2·80	3·48	3·47	3·48
K_2O	0·15	0·15	0·44	0·17	0·17	0·11	0·12	0·17	0·11	0·14	0·11
P_2O_5	0·27	0·27	0·31	0·28	0·37	0·27	0·27	0·28	0·26	0·27	0·27
H_2O	0·28	0·25	n.d.	0·24	0·26	n.d.	0·23	0·21	n.d.	n.d.	n.d.
Total	99·02	98·99	98·78	98·94	100·38	99·23	99·43	100·11	99·54	98·84	98·72
mg-no.	66·01	67·13	71·31	64·82	59·15	65·02	64·53	62·85	65·37	64·58	65·03
Trace elements (ppm)											
Sc	29·1		34·5	31·3	37·7	29·1		30·0			
Cr	278		305	252	198	253		255			
Co	38·9		36·3	36·7	36·5	36·9		37·8			
Ni	104		76·1	84·8	90·8	86·0		96·0			
Cu	52·5		64·7	47·1	47·0	53·7		48·2			
Zn	86·5		90·3	86·3	97·9	79·4		82·5			
Ga	15·1		15·3	16·1	17·9	14·9		15·5			
Rb	2·15		1·19	2·68	2·03	1·26		2·59			
Sr	84·9		127	118	120	136		100			
Y	25·7		27·8	30·5	43·0	25·0		28·7			
Zr	66·9		94·3	98·1	156	90·2		82·4			
Nb	2·67		2·26	3·23	3·47	1·87		3·11			
Cs	0·013		0·021	0·017	0·033	0·000		0·012			
Ba	19·9		15·1	20·8	21·7	11·5		22·4			
La	2·85		2·98	3·97	5·07	3·26		3·45			
Ce	8·31		9·22	12·0	15·4	10·8		10·3			
Pr	1·45		1·69	2·07	2·78	1·95		1·80			
Nd	7·98		8·97	11·1	14·6	10·2		9·66			
Sm	2·98		3·15	3·91	5·14	3·41		3·48			
Eu	1·05		1·15	1·35	1·70	1·25		1·23			
Gd	4·09		4·18	5·11	6·60	4·39		4·72			
Tb	0·760		0·762	0·923	1·21	0·772		0·863			
Dy	5·21		4·99	6·27	8·00	5·18		5·90			
Ho	1·09		1·07	1·28	1·71	1·06		1·22			
Er	3·07		3·00	3·64	4·87	2·92		3·46			
Tm	0·455		0·436	0·535	0·719	0·430		0·511			
Yb	3·02		2·86	3·55	4·66	2·83		3·39			
Lu	0·437		0·422	0·524	0·694	0·409		0·494			
Hf	2·39		2·48	3·25	4·26	2·81		2·88			
Ta	0·165		0·154	0·202	0·210	0·119		0·193			
Tl	n.d.		0·013	n.d.	0·018	n.d.		n.d.			
Pb	0·388		0·588	0·636	0·742	0·705		0·465			
Th	0·188		0·138	0·211	0·236	0·116		0·202			
U	0·062		0·054	0·075	0·092	0·039		0·064			

Table 1: continued

Segment:	E7	E7	E7	E7	E7	E7	E7	E7	E7	E8	E8
Sample:	109DS-7	110DS-1	110DS-2	110DS-3	110DS-4	110DS-5	110DS-6	110DS-7	wx55	wx56	wx57
Lat. (S):	58°36·6′	58°44·2′	58°44·2′	58°44·2′	58°44·2′	58°44·2′	58°44·2′	58°44·2′	58°49·88′	58°49·81′	59°01·82′
Long. (W):	29°57·7′	29°56·0′	29°56·0′	29°56·0′	29°56·0′	29°56·0′	29°56·0′	29°56·0′	29°52·15′	29°37·17′	29°31·20′
Depth (m):	3636	3916	3916	3916	3916	3916	3916	3916	3260	3587	3364
Major elements (wt %)											
*n*ME/*n*H_2O	25	21	15/3	20	15	19/3	11/3	13	6	16	28/2
SiO_2	50·78	50·83	50·70	50·66	51·17	50·89	51·49	51·24	51·36	53·09	51·26
TiO_2	1·60	1·96	1·94	1·97	1·95	1·95	1·94	1·97	1·46	1·72	1·59
Al_2O_3	15·13	14·67	14·97	14·52	15·03	14·97	15·07	15·00	14·75	15·21	15·00
FeO	9·45	10·03	9·39	9·93	9·35	9·36	9·25	9·36	8·95	9·98	9·56
MnO	0·20	0·20	0·19	0·19	0·19	0·18	0·18	0·19	0·20	0·19	0·20
MgO	7·57	6·86	6·98	6·81	6·96	6·94	7·02	6·95	7·58	5·04	7·40
CaO	11·39	10·99	10·95	11·02	10·94	10·97	10·89	10·98	11·83	9·49	11·41
Na_2O	2·79	2·93	2·95	2·98	2·95	2·96	2·97	2·97	3·18	3·55	3·37
K_2O	0·17	0·26	0·26	0·27	0·25	0·27	0·25	0·26	0·25	0·21	0·15
P_2O_5	0·28	0·35	0·35	0·32	0·37	0·34	0·36	0·36	0·28	0·31	0·32
H_2O	n.d.	n.d.	0·33	n.d.	n.d.	0·35	0·40	n.d.	n.d.	n.d.	0·26
Total	99·35	99·08	99·01	98·67	99·17	99·19	99·82	99·29	99·82	98·79	100·51
mg-no.	62·69	58·94	60·92	58·98	60·96	60·86	61·41	60·91	64·00	51·45	61·88
Trace elements (ppm)											
Sc				27·2					37·7	35·4	37·8
Cr				204					251	27·9	262
Co				30·5					38·3	31·8	37·7
Ni				68·7					87·0	26·8	85·3
Cu				39·2					62·0	56·4	60·4
Zn				95·1					126	84·0	76·0
Ga				13·8					17·0	17·3	16·1
Rb				3·76					1·91	2·67	1·39
Sr				95·6					125	143	151
Y				28·6					32·0	32·2	30·7
Zr				95·2					107	121	112
Nb				3·92					2·49	2·71	2·32
Cs				0·027					0·049	0·058	0·021
Ba				29·9					17·2	28·6	16·3
La				4·37					3·39	4·17	3·76
Ce				12·4					10·5	12·3	11·3
Pr				2·10					1·87	2·15	1·99
Nd				10·7					10·1	11·2	10·4
Sm				3·62					3·59	3·75	3·58
Eu				1·22					1·26	1·34	1·30
Gd				4·78					4·76	4·91	4·62
Tb				0·870					0·874	0·891	0·849
Dy				5·90					5·84	5·88	5·59
Ho				1·23					1·26	1·26	1·19
Er				3·48					3·58	3·59	3·41
Tm				0·519					0·524	0·527	0·497
Yb				3·46					3·43	3·50	3·24
Lu				0·502					0·506	0·528	0·481
Hf				3·16					2·88	3·13	2·89
Ta				0·227					0·223	0·157	0·150
Tl				0·001					0·020	0·021	0·015
Pb				0·594					0·936	0·705	0·577
Th				0·264					0·165	0·219	0·159
U				0·090					0·062	0·080	0·061

Segment:	E8	E8	E8	E8	E8	E9	E9	E9	E9	E9	E9
Sample:	wx58	wx59	wx60	wx61	wx62	wx63	wx64	wx65	wx67	wx66	wx66dupl.
Lat. (S):	59°10·23′	59°16·81′	59°19·21′	59°25·19′	59°37·18′	59°32·99′	59°46·74′	59°55·20′	60°03·25′	60°04·25′	60°04·25′
Long. (W):	29°30·08′	29°30·60′	29°30·29′	29°30·01′	29°33·00′	30°04·79′	30°04·80′	30°01·21′	29°58·21′	29°58·01′	29°58·01′
Depth (m):	3356	2816	2705	3148	3764	3237	3346	2849	2694	2442	2442
Major elements (wt %)											
*n*ME/*n*H_2O	10/7	10	13	6	11	19	10	18/5	16/5	23/4	
SiO_2	51·53	56·53	54·98	54·86	52·31	52·11	50·99	51·75	51·53	51·30	
TiO_2	1·64	1·14	1·69	0·88	0·89	1·24	1·12	0·90	1·85	1·53	
Al_2O_3	14·93	14·74	15·16	15·67	16·36	16·34	15·97	16·40	15·71	15·78	
FeO	9·78	9·89	10·78	8·96	8·07	8·20	7·86	7·48	9·13	8·83	
MnO	0·20	0·20	0·22	0·18	0·17	0·18	0·18	0·17	0·17	0·18	
MgO	7·16	4·26	3·58	5·63	6·65	6·20	6·94	7·06	6·61	7·21	
CaO	11·31	8·54	7·67	10·19	11·80	10·95	11·61	12·03	10·57	11·32	
Na_2O	3·37	3·06	3·49	2·56	2·50	3·21	3·05	2·68	3·77	3·62	
K_2O	0·16	0·28	0·21	0·21	0·13	0·27	0·28	0·21	0·52	0·30	
P_2O_5	0·31	0·26	0·28	0·25	0·26	0·29	0·29	0·26	0·40	0·34	
H_2O	0·24	n.d.	n.d.	n.d.	n.d.	n.d.	n.d.	0·92	0·44	0·30	
Total	100·64	98·90	98·06	99·39	99·13	99·00	98·28	99·85	100·71	100·71	
mg-no.	60·58	47·47	41·08	56·85	63·36	61·33	64·92	66·44	60·31	63·16	
Trace elements (ppm)											
Sc	37·5	36·0	33·6	37·0	37·0	31·3	26·3	33·8	35·7	38·6	40·4
Cr	238	23·2	12·4	70·1	223	158	202	224	197	190	255
Co	37·3	31·8	34·1	31·6	33·2	32·6	36·2	31·8	34·4	35·7	35·7
Ni	91·1	18·7	19·1	35·8	61·8	69·3	104	84·7	64·8	63·1	61·8
Cu	62·2	115	69·7	95·0	74·8	62·8	65·8	64·5	53·6	70·6	64·6
Zn	73·4	78·2	73·3	66·7	60·1	64·3	60·3	45·7	83·2	83·4	57·5
Ga	15·5	15·5	15·7	14·1	13·6	14·8	13·7	12·8	17·7	17·3	15·4
Rb	1·43	3·38	2·20	2·83	1·48	3·95	2·28	2·78	8·75	4·48	4·40
Sr	140	143	138	135	124	160	171	155	221	185	184
Y	27·2	21·4	20·8	16·2	16·1	21·5	16·0	14·1	33·0	25·6	25·9
Zr	95·3	68·0	62·8	48·1	43·9	85·6	70·7	46·0	163	82·0	105·0
Nb	2·03	1·60	1·43	0·947	0·767	3·52	3·47	2·04	8·88	4·49	5·15
Cs	0·027	0·117	0·074	0·082	0·054	0·087	0·046	0·060	0·141	0·076	0·068
Ba	15·3	46·4	35·3	32·0	26·5	51·7	67·6	31·8	90·0	51·7	49·4
La	3·15	2·67	2·24	2·08	1·53	3·90	3·28	2·52	8·46	5·82	5·43
Ce	9·65	7·80	6·88	5·99	4·75	10·5	8·70	6·70	21·0	15·0	14·8
Pr	1·68	1·33	1·22	1·00	0·854	1·71	1·38	1·09	3·21	2·27	2·34
Nd	8·94	6·80	6·53	5·27	4·67	8·58	6·91	5·54	15·3	11·3	11·6
Sm	3·06	2·32	2·25	1·77	1·70	2·68	2·21	1·78	4·54	3·49	3·62
Eu	1·15	0·864	0·882	0·720	0·686	0·981	0·846	0·715	1·58	1·29	1·29
Gd	4·09	3·04	3·04	2·39	2·28	3·34	2·69	2·31	5·44	4·40	4·48
Tb	0·745	0·554	0·562	0·439	0·426	0·606	0·480	0·404	0·960	0·775	0·776
Dy	4·89	3·74	3·73	2·93	2·84	3·96	3·13	2·67	6·12	5·04	5·11
Ho	1·05	0·801	0·816	0·641	0·613	0·844	0·648	0·567	1·29	1·06	1·07
Er	2·99	2·31	2·32	1·85	1·79	2·34	1·83	1·68	3·56	3·19	3·16
Tm	0·444	0·350	0·345	0·276	0·265	0·347	0·263	0·232	0·517	0·437	0·432
Yb	2·89	2·32	2·32	1·83	1·77	2·27	1·70	1·52	3·37	2·90	2·79
Lu	0·432	0·359	0·341	0·275	0·262	0·340	0·251	0·227	0·493	0·420	0·410
Hf	2·41	1·78	1·73	1·34	1·23	2·24	1·78	1·33	3·95	2·92	2·92
Ta	0·128	0·115	0·098	0·058	0·048	0·227	0·218	0·127	0·533	0·304	0·324
Tl	0·015	0·029	0·019	0·024	0·015	0·029	0·019	0·015	0·030	0·019	0·019
Pb	0·556	0·888	0·682	0·886	0·566	1·70	0·628	0·568	0·995	0·670	0·673
Th	0·140	0·281	0·166	0·220	0·121	0·305	0·253	0·193	0·610	0·319	0·316
U	0·051	0·089	0·053	0·067	0·038	0·110	0·091	0·067	0·220	0·120	0·124

Table 1: continued

Segment:	E9	E9	Standards	S.D.	Standards	S.D.
Sample:	wx68	wx69	JDF-D2		CFA47-2	
Lat. (S):	60°12·00′	60°20·01′				
Long. (W):	29°52·19′	29°42·58′				
Depth (m):	2817	3259				
Major elements (wt %)						
*n*ME/*n*H_2O	20/5	19/9	$n = 17$	$n = 28$		
SiO_2	51·29	51·33	50·62	0·74	61·47	0·47
TiO_2	1·71	1·58	1·91	0·05	0·43	0·04
Al_2O_3	14·71	15·67	13·70	0·19	18·57	0·20
FeO	9·61	8·69	12·02	0·41	2·72	0·08
MnO	0·21	0·18	0·23	0·03	0·18	0·04
MgO	6·66	7·22	6·61	0·10	0·41	0·02
CaO	11·26	11·02	10·79	0·13	1·83	0·15
Na_2O	3·64	3·50	2·79	0·03	5·33	0·05
K_2O	0·33	0·37	0·21	0·02	7·92	0·09
P_2O_5	0·34	0·33	0·33	0·03	0·11	0·03
H_2O	0·31	0·34				
Total	100·06	100·24	99·21		98·97	
mg-no.	59·22	63·54				
Trace elements (ppm)			BHVO-1 ($n = 3$)		BIR ($n = 3$)	
Sc	38·9	32·9	30·5	2·77	43·0	1·69
Cr	151	200	277	11·16	365	10·99
Co	37·6	34·0	42·8	0·91	50·2	0·21
Ni	57·0	72·0	114	2·5	165	2·93
Cu	66·2	59·0	133	5·07	113	2·54
Zn	82·0	76·0	107	7·06	72·2	8·63
Ga	17·0	16·5	21·3	0·40	15·1	0·04
Rb	4·96	6·22	9·39	1·79	0·31	0·01
Sr	177	189	402	7·91	110	2·58
Y	29·7	27·6	24·4	0·98	14·4	0·62
Zr	123	128	179	15·61	15·2	1·20
Nb	5·38	6·04	16·8	0·57	0·535	0·01
Cs	0·076	0·100	0·108	0·01	0·007	0·000
Ba	53·4	65·4	133	1·75	6·53	0·20
La	5·67	6·23	14·9	0·29	0·633	0·01
Ce	14·9	15·7	35·6	1·22	1·84	0·03
Pr	2·43	2·49	5·27	0·11	0·376	0·004
Nd	12·1	12·0	23·8	0·25	2·31	0·05
Sm	3·85	3·73	6·03	0·06	1·13	0·04
Eu	1·39	1·32	2·02	0·004	0·505	0·001
Gd	4·73	4·54	6·00	0·06	1·76	0·02
Tb	0·858	0·805	0·937	0·01	0·357	0·01
Dy	5·51	5·20	5·22	0·14	2·53	0·04
Ho	1·17	1·09	0·982	0·02	0·56	0·005
Er	3·29	3·06	2·45	0·03	1·63	0·01
Tm	0·481	0·444	0·323	0·003	0·247	0·002
Yb	3·13	2·90	1·97	0·03	1·63	0·01
Lu	0·456	0·428	0·276	0·004	0·246	0·002
Hf	3·12	3·10	4·64	0·17	0·595	0·04
Ta	0·329	0·355	1·02	0·04	0·039	0·001
Tl	0·024	0·021	0·045	0·01	0·009	0·01
Pb	0·733	0·786	1·99	0·03	2·99	0·04
Th	0·381	0·448	1·16	0·04	0·031	0·000
U	0·132	0·152	0·416	0·01	0·011	0·01

wx, samples recovered by wax coring on cruise JR39b; DS, samples dredged on cruise PS47; *n*ME, number of major element analyses; *n*H_2O, number of FTIR analyses; n.d., not detected.

Table 2: Sr–Nd–Pb isotope ratios of the East Scotia Ridge volcanic glasses analysed by TIMS

Segment	Sample	$^{87}Sr/^{86}Sr$	±	$^{143}Nd/^{144}Nd$	±	$^{206}Pb/^{204}Pb$	±	$^{207}Pb/^{204}Pb$	±	$^{208}Pb/^{204}Pb$	±
E3	96DS-1	0·702583	5	0·513104	6	18·047	4	15·475	3	37·578	8
E3	wx45	0·702636	7	0·513098	8	18·007	2	15·482	2	37·581	5
E3	97DS-1	0·702666	7	0·513101	11	18·039	2	15·487	2	37·652	4
E3	wx46	0·703035	8	0·513042	9	18·163	1	15·512	1	37·886	3
E3	98DS-1	0·703122	7	0·513023	13	18·206	3	15·523	2	37·973	5
E4	wx47	0·703288	8	0·513004	7	18·255	1	15·530	1	38·051	2
E4	99DS-1	0·703481	6	0·512915	6	18·463	2	15·587	2	38·405	5
E4	99DS-4	0·703497	5	0·512923	7	18·453	2	15·570	1	38·359	4
E4	100DS-1	0·702768	7	0·513067	8	18·093	2	15·507	2	37·743	5
E5	wx48	0·702511	9	0·513121	5	18·025	4	15·496	3	37·571	8
E5	104DS-1	0·702554	8	0·513105	7	18·072	1	15·483	1	37·607	3
E5	wx49	0·702489	7	0·513113	4	17·999	5	15·477	4	37·515	9
E5	wx50	0·702540	8	0·513075	9	18·083	2	15·474	2	37·574	4
E6	106DS-1	0·702622	6	0·513129	7	17·832	3	15·463	3	37·399	7
E6	107DS-1	0·702498	9	0·513111	11	17·838	2	15·463	1	37·370	4
E6	107DS-3	0·702749	7	0·513112	7	17·904	3	15·476	2	37·517	6
E6	108DS-1	0·702824	7	0·513084	8	17·871	2	15·475	2	37·465	5
E7	wx54b	0·702649	8	0·513120	5	17·869	7	15·497	6	37·514	14
E7	109DS-1	0·702517	8	0·513143	4	17·869	4	15·450	3	37·391	8
E7	110DS-3	0·702829	7	0·513081	6	17·885	4	15·473	3	37·506	8
E8	wx56	0·702807	8	0·513105	8	17·946	2	15·484	2	37·619	5
E8	wx60	0·702911	9	0·513101	6	18·231	3	15·537	3	38·010	6
E8	wx62	0·702869	9	0·513072	5	18·276	2	15·535	2	38·035	4
E9	wx63	0·702982	8	0·513034	7	18·213	2	15·539	2	37·984	5
E9	wx64	0·703038	8	0·513031	7	18·091	5	15·517	4	37·821	10
E9	wx65	0·703039	9	0·513009	9	18·198	2	15·548	2	38·010	5
E9	wx67	0·703102	8	0·513001	9	17·992	3	15·505	2	37·675	6
E9	wx68	0·702940	10	0·513063	7	17·919	7	15·487	6	37·590	14
E9	wx69	0·703100	7	0·513016	8	17·935	2	15·513	2	37·659	4

± 11 (n = 11) over the course of this study. The long-term reproducibility of NBS 981 (n = 63) in this laboratory is $^{206}Pb/^{204}Pb$ = 16·896 ± 5, $^{207}Pb/^{204}Pb$ = 15·437 ± 7 and $^{208}Pb/^{204}Pb$ = 36·524 ± 21. During the course of this study, NBS 981 analyses (n = 8) gave $^{206}Pb/^{204}Pb$ = 16·893 ± 10, $^{207}Pb/^{204}Pb$ = 15·433 ± 13 and $^{208}Pb/^{204}Pb$ = 36·514 ± 41, and were corrected to the values of Todt *et al.* (1996). Total chemistry Pb blanks were <0·3 ng and thus negligible. In Table 2 we show the isotope analyses of selected East Scotia Ridge samples and the 2σ standard deviations.

RESULTS

Petrography and mineral chemistry

We present a general summary of the major petrographic features and mineralogical characteristics of the dredged lavas from segments E3–E7 in Table 3. Individual mineral analyses are not presented here, but can be downloaded from the *Journal of Petrology* Web site at http://www.petrology.oupjournals.org. The phenocrysts are dominated by plagioclase and olivine phenocrysts with subordinate clinopyroxene, chrome spinel and magnetite. The most visible differences between the samples are in both their phenocryst contents and their vesicularity. Samples from segment E3 (96DS, 97DS, 98DS) contain some plagioclase and olivine phenocrysts (5%) and few vesicles, whereas the lavas from segment E4 (99DS, 100DS) are highly vesicular, but have an almost aphyric groundmass and sparse olivine and plagioclase phenocrysts (<3%). Most of the samples from dredge locations in segments E5 (104DS), E6 (106DS, 107DS) and E7 (109DS, 110DS) are slightly vesicular and exhibit a far higher plagioclase phenocryst content (30%) than the other segments.

Table 3: Petrographic description of the dredged samples

Segment	Sample	Rock description
E3	96DS-1	tube lava with glassy rim (up to 1 cm thick), slightly vesicular, few olivine and feldspar phenocrysts
	96DS-2	lava fragment with glassy rim (up to 1 cm thick), few small vesicles, few feldspar phenocrysts
	96DS-3	small piece of lava with ropy surface, glassy rim with devitrification, oxidation on the ropy surface, few feldspar phenocrysts
	96DS-4	small piece of lava, glassy rim (0·5 cm), devitrification, slightly vesicular, few feldspar phenocrysts
	97DS-1	glass-rimmed piece, aphyric with rare patches of feldspar phenocrysts
	97DS-2	small basaltic pillow, glass rimmed (0·5 cm), feldspar phenocrysts up to 6 mm, fractured interior, devitrified glass, alteration beneath glass
	97DS-3	glassy fragment, rare feldspar microphenocrysts, initial stage of devitrification
	97DS-4	glassy fragment, 10% devitrification on base
	97DS-5	small pillow with glassy rim (0·2 cm), 15–20% devitrification, strongly feldspar phyric (up to 0·5 cm)
	98DS-1	large piece of a pillow, glassy rim up to 0·5 cm, slightly vesicular, some vesicles glass-coated, some feldspar phenocrysts
E4	99DS-1	pillow fragment with thin glass crust, vesicles (up to 1 cm), aphyric
	99DS-2	inner part of a pillow, large vesicles (up to 2 cm), aphyric
	99DS-3	pillow, vesicle-rich, some tube-formed (up to 2 cm), glassy rim (up to 1 cm thick), aphyric
	99DS-4	glassy piece of sheet flow, aphyric
	100DS-1	pillow fragment with glass crust, slightly vesicular (mm size)
E5	102DS-1	small fragment with glassy rim with pervasive devitrification, feldspar microphenocrysts in less glassy material
	104DS-1	large basaltic block with 0·8 cm thick glass rim (aphyric), interior is strongly feldspar-phyric (15%)
	104DS-3	lava tube fragment with glassy rim (0·8 cm), glass and interior contain feldspar phenocrysts
E6	106DS-1	pillow fragment with glassy rim (up to 1 cm thick), Fe hydroxide alteration on fracture planes
	106DS-2	piece of pillow with thin glass rim, fresh dark grey colour, feldspar phenocrysts
	106DS-3	thick glassy piece, slightly altered with brownish grey colour
	106DS-4	piece of pillow with glassy rim (up to 0·5 cm) alterated fracture planes with Fe hydroxides, inner parts of rock free of alteration, some feldspar phenocrysts
	107DS-1	pillow fragment with glassy rim (up to 1 cm thick), aphyric, slightly vesicular, rare feldspar phenocrysts
	107DS-3	glass-rimed (up to 0·5 cm thick) lava piece, slightly vesicular, aphyric
	107DS-4	glass-rimmed (up to 1 cm) lava fragment, slightly vesicular, aphyric
	108DS-1	small fragment of weakly devitrified, aphyric glass
E7	109DS-1	piece of lava tube, glassy rim (0·3 cm), aphyric
	109DS-2	glass-rimmed (up to 0·5 cm) weakly vesicular flow fragment
	109DS-3	glassy crust, aphyric with small vesicles
	109DS-4	lava tube fragment with glassy rim (0·3 cm), aphyric
	109DS-5	see 109DS-4
	109DS-6	see 109DS-4
	109DS-7	flow fragment slightly glassy and vesicular, Fe hydroxide staining
	110DS-1	pillow lava lobe with glassy rim (0·6 cm), slightly vesicular interior, weakly feldspar phyric
	110DS-2	pillow fragment weakly devitrified glass rim (0·5 cm), slightly vesicular interior, aphyric
	110DS-3	lava fragment with ropy surface structure, thin glass crust, interior slightly vesicular, aphyric
	110DS-4	see 110DS-3
	110DS-5	similar to 110DS-3, but more channelled surface—almost ropy
	110DS-6	piece of lava tube with glassy rim (up to 0·3 cm thick), contains rare feldspar phenocrysts
	110DS-7	see 110DS-6

Olivine phenocrysts are mostly rounded or highly skeletal crystals. Subordinate olivine is present in the matrix and glass rims. Generally, individual olivine phenocrysts show a comparable range of Fo_{89} (cores) to Fo_{83} (rims). There are no distinct chemical differences between phenocrysts and matrix minerals. Calculations show that most olivines are in equilibrium with the matrix glass at atmospheric pressure for a Fe/Mg K_D of 0·3 (Roeder & Emslie, 1970; Ulmer, 1989).

Plagioclase phenocrysts are up to 5 mm long in volcanic rocks from segments E5–E7 and with smaller sizes of up to 2 mm in the lavas of segments E3 and E4. Some phenocrysts show zonation from calcic cores to more sodic rims. Core compositions fall in the range $An_{92–85}$ and rims, as well as unzoned phenocrysts, have An contents of 78–87. Matrix plagioclase crystals are the least calcic with the range $An_{70–82}$.

Generally, opaque minerals are scarce in East Scotia Ridge lavas. Titanomagnetite, magnetite and chrome spinels mostly form inclusions in olivine phenocrysts in the lavas of segments E3 and E4. The *cr*-number in the spinels ranges from 62 to 66.

Magmatic geochemistry

Major element analyses of the dredged and wax core samples are presented in Table 1. Figure 3 shows all the East Scotia Ridge lavas as well as the chemical trends of the subduction-related magmas from the South Sandwich Islands in the K_2O–SiO_2 classification diagram of Peccerillo & Taylor (1976). The majority of the back-arc samples range from basalt to basaltic andesite and are primarily low-K tholeiites, although some show medium-K compositions. For a given SiO_2 abundance, samples from segments E2 and E4 are significantly enriched in K_2O relative to the other segments. MgO contents for the majority of segments lie in the restricted range of 6–9 wt % and have *mg*-number between 60 and 70. However, segments E2 and E8 have yielded samples with MgO contents as low as 3 wt % and with *mg*-number as low as 40. These two segments also show systematic variations of CaO with MgO (Fig. 4a). In the plot of Al_2O_3 against MgO, each segment forms a distinct trend, parallel to those from the other segments and to the Mid-Atlantic Ridge (Fig. 4b).

Water contents of selected East Scotia Ridge magmas cover the range of 0·2–2·3 wt % (Table 1). Water contents of MORB vary between 0·05 and 1·3 wt % (Michael, 1995), although most N-MORB have contents between 0·1 and 0·4 wt % (Michael & Chase, 1987; Dixon *et al.*, 1988; J. E. Dixon, personal communication, 2001). All samples from East Scotia Ridge segments E6 and E7 show H_2O contents within this N-MORB range. Some samples from segments E2, E3, E4 and E9, however, contain up to 2·2 wt % H_2O (Table 1). It was not possible to measure the H_2O content of all the volcanic glasses along the back-arc, because of the presence of vesicles and microcrystals. We measured the H_2O content of only two E2 samples from the centre of the segment (WX42, WX43; Table 1).

Selected volcanic glass samples were analysed for trace elements and compositions are listed in Table 1. Comparison of the relative abundances of highly and moderately incompatible trace elements along the East Scotia Ridge is facilitated by using N-MORB-normalized (Hofmann, 1988) abundance profiles (Fig. 5). Relative to N-MORB, the East Scotia Ridge volcanic glasses have higher abundances of large ion lithophile elements (LILE) such as K, Pb, Rb and Ba, but are less enriched than bulk South Atlantic sediment (from Plank & Langmuir, 1998). In contrast, the bulk sediment pattern has lower HREE abundances than the back-arc magmas. Trace element patterns of the South Sandwich Islands samples are sub-parallel to those of the back-arc glasses, although the island arc magmas tend to be more depleted in Nb, Ta, Zr and Hf.

Isotopic data for selected East Scotia Ridge samples are given in Table 2. The back-arc magmas are less radiogenic in terms of Sr and Pb than those from the South Sandwich Islands (for discussion, see section on components contributing to the back-arc source and Figs 15 and 16) and in the case of segments E6 and E7 show isotopic ratios as low as an average MORB (from Cohen & O'Nions, 1982*b*). The Nd isotopic ratios of the back-arc magmas are comparable with those from the island arc. Both island arc and back-arc are much less radiogenic in Sr and more radiogenic in Nd compared with bulk South Atlantic sediment. The Pb isotopes in the sediments are similar to those in the island-arc magmas and lie at the radiogenic extreme of the back-arc magma fields.

MODELLING FRACTIONAL CRYSTALLIZATION

The large range of major element compositions covered by the samples from segments E2 and E8 (see, for example, Figs 3 and 4) can be modelled at least partially as the product of simple crystal fractionation. Unfortunately, as these segments were sampled only with a wax corer, it is impossible to check our results against the petrography of the lavas. We have performed crystal fractionation calculations using the least-squares GPP program of Geist *et al.* (1989) and mineral compositions measured on phenocrysts from other segments. The calculated fractionation trends are shown in the CaO vs MgO diagram (Fig. 4a), together with the mineral contents of the cumulate. The trends can be modelled as the result of either one- (E2) or two-stage (E8) crystal

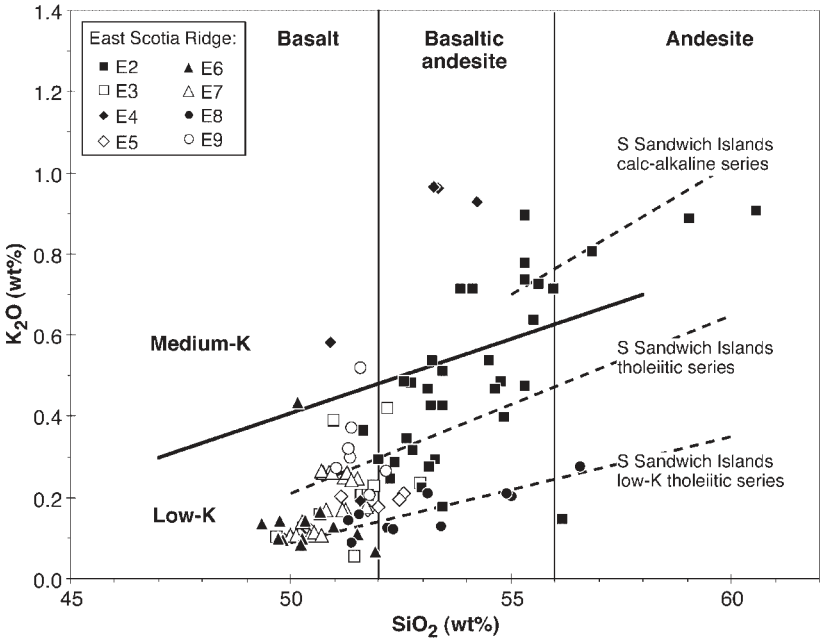

Fig. 3. K_2O vs SiO_2 diagram for volcanic glasses from the East Scotia Ridge. Data for the E2 segment samples are, apart from WX42–WX44 (Table 1), from Leat *et al.* (2000). Generalized trends for the low-K tholeiite, tholeiite and calc-alkaline series from the South Sandwich island arc (Pearce *et al.*, 1995) are indicated by dashed lines. Series boundaries and nomenclature from Peccerillo & Taylor (1976).

fractionation. Olivine, plagioclase, and subordinate chrome spinel can produce the trend between 9 and 7 wt % MgO in the E8 magmas, whereas below 7 wt % MgO the decrease in CaO in both E2 and E8 reflects the appearance of clinopyroxene in the fractionating assemblage.

One of the most differentiated glass samples of segment E2 (WX33, Leat *et al.*, 2000) could be produced from the assumed parental basalt (WX21, Leat *et al.*, 2000) by a total of ~50% fractional crystallization: 27·3% clinopyroxene, 20·8% plagioclase, 2·4% olivine, 0·5% chrome spinel ($R^2 = 0{\cdot}24$). The first step fractionation model for samples from segment E8 yielded ~10% crystal fractionation from the assumed parental (WX58) to daughter magma composition (WX62): 5% plagioclase, 3·5% olivine, 0·8% chrome spinel ($R^2 = 0{\cdot}33$). During the second step fractionation, the most differentiated glass sample of segment E8 (WX60) could be produced by ~40% fractional crystallization: 19·5% plagioclase, 17·5% clinopyroxene, 4·4% olivine, 0·1% chrome spinel ($R^2 = 0{\cdot}11$).

It is important to note that elevated water contents increase the mineral–liquid K_d of plagioclase and suppress plagioclase crystallization (e.g. Eggler & Burnham, 1973; Michael & Chase, 1987; Sisson & Grove, 1993; Hergt & Farley, 1994). At present, these effects cannot be quantified in a rigorous way and so the calculations discussed above should only be taken as indicative of the fractional crystallization processes that may have affected the lavas.

The East Scotia Ridge lavas have high Al_2O_3 for a given MgO content compared with the Mid-Atlantic Ridge (MAR) glasses (Fig. 4b). High Al_2O_3 concentrations compared with MORB have also been observed in other back-arc regions (e.g. Mariana Trough, Sumisu–Torishima back-arc rifts) and have been attributed to the greater H_2O content in back-arc magmas during crystallization (Sinton & Fryer, 1987; Fryer *et al.*, 1990). The differences in Al_2O_3 contents between segments shown in Fig. 4b may reflect either the effect of varying amounts of water on plagioclase crystallization or differences in Al_2O_3 contents of magmas in different segments. Experimental work (Gaetani & Grove, 1998) has shown that varying amounts of water in the source at the time of melting will not affect the Al content of the primary magma and so an investigation of the relationship between Al and H_2O in the magmas should be able to distinguish between these two possibilities. Moreover, the measured H_2O content of the glasses should reflect unperturbed magmatic values, as degassing during ascent and eruption has little effect on dissolved H_2O contents unless eruption depths are less than a few hundred metres (e.g. Stolper & Newman, 1994). This is confirmed for the East Scotia Ridge by our observations that there is no correlation between eruption depth and measured water contents in the glasses.

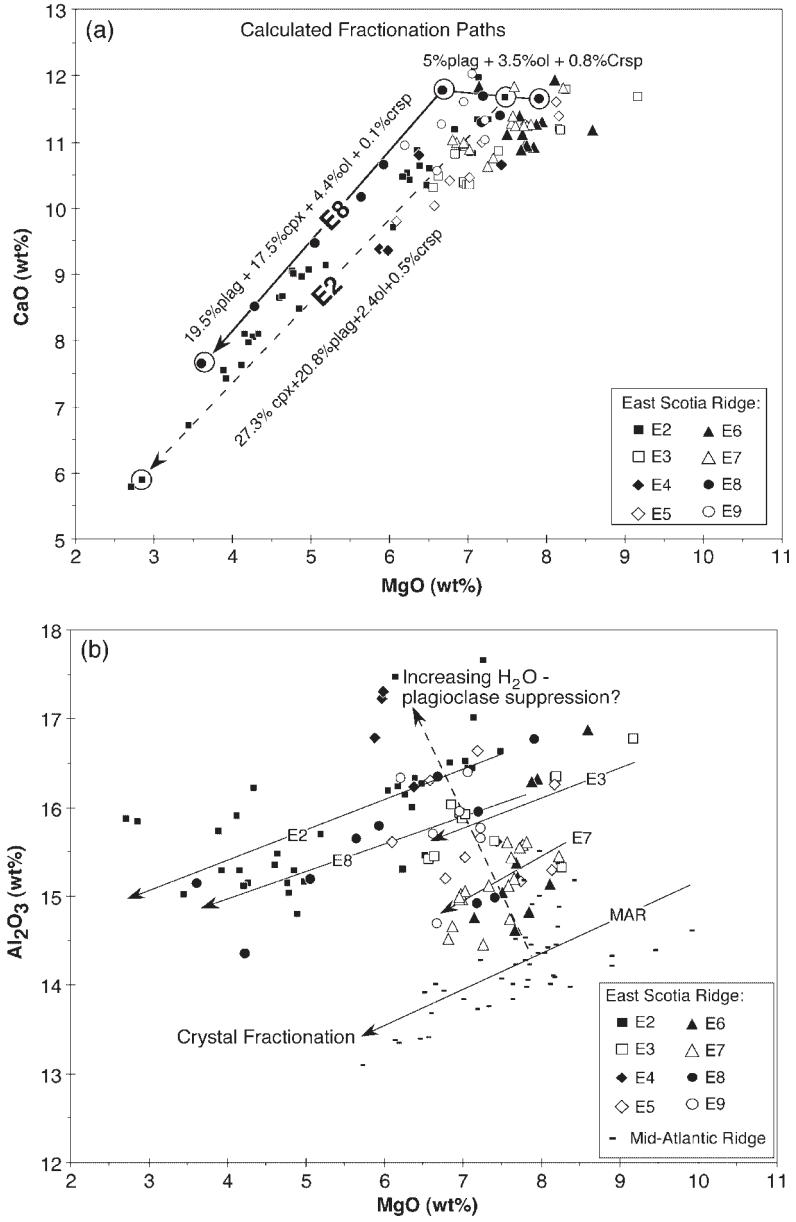

Fig. 4. Variation of CaO and Al_2O_3 (wt %) vs wt % MgO for samples from the East Scotia Ridge. In (a), the continuous and dashed lines represent calculated liquid compositions from crystal fractionation models determined with the GPP program of Geist *et al.* (1985). In (b), the continuous lines with arrows show the crystal fractionation trends of the E2 (Leat *et al.*, 2000), E3, E7 and E8 segments, and Mid-Atlantic Ridge lavas (MAR: Schilling *et al.*, 1983). Each segment forms a distinct trend, parallel to those from the other segments and to the Mid-Atlantic Ridge. The dashed line with an arrow is perpendicular to the fractionation trends and may reflect either the effect of varying amounts of water on plagioclase crystallization or different Al_2O_3 contents in primary magmas of each segment (see text for details).

First, however, we must remove the effects of low-pressure crystal fractionation on Al_2O_3 and H_2O in the erupted magmas. For Al_2O_3, this involves calculating Al_8 (Al_2O_3 content of the magma recalculated to 8 wt % MgO along the fractionation vector for each segment) in a manner similar to the Fe_8 or Na_8 values of Klein & Langmuir (1987). We chose samples for H_2O determinations that are relatively primitive (>6% MgO), and so do not expect the effects of crystal fractionation on water contents to be large. We used the quantified fractionation assemblages calculated above and the Rayleigh distillation equation (see, e.g. Cox *et al.*, 1979) to work out the effects of fractionation on magmatic water contents, assuming complete incompatibility of water in the cumulate assemblage. Figure 6 shows the relationship between $(H_2O)_8$ and Al_8. We see a positive correlation

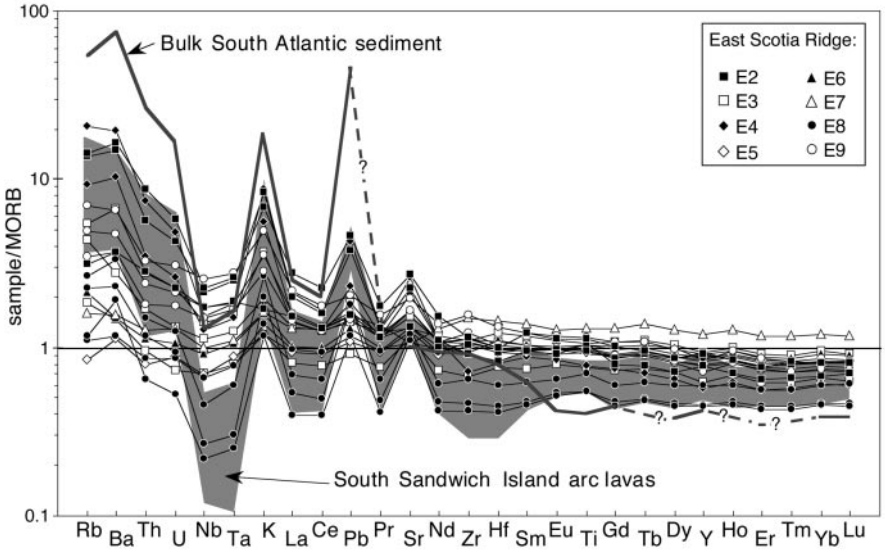

Fig. 5. N-MORB-normalized (Hofmann, 1988) trace element patterns for selected volcanic glasses from the East Scotia Ridge. Data for the E2 segment (apart from WX42–WX44) are from Leat *et al.* (2000) and the shaded area represents the range of trace element abundances in South Sandwich island arc lavas (Pearce *et al.*, 1995). The thick continuous line represents the composition for bulk South Atlantic sediment ($n = 15$) from Plank & Langmuir (1998).

between these two parameters which, in view of the possibilities outlined above, we interpret as reflecting the effect of magmatic water content on plagioclase solubility in the melt. Michael & Chase (1987) have shown that the MORB crystallization sequence is olivine → olivine + plagioclase → olivine + plagioclase + clinopyroxene. Our interpretation of the correlation between $(H_2O)_8$ and Al_8 is that magmas with higher water contents progress further along the olivine-only fractionation path (shown in Fig. 4b) and so reach higher Al_2O_3 contents before plagioclase starts to precipitate.

In general, segments E2 and E8 are most strongly affected by fractional crystallization processes, with differentiated samples reaching MgO contents as low as 3 wt %. Interestingly, the samples with lowest MgO concentrations erupt near the topographic highs at the centres of these two segments. Surprisingly, lavas of segment E9, which shows a very pronounced topographic high, are not strongly fractionated. Geophysical investigations of segment E2 (Livermore *et al.*, 1997) showed that there is a melt lens situated directly beneath the topographic high at the segment centre, ~3 km beneath the sea floor. Leat *et al.* (2000) suggested that the highly fractionated magmas observed on the high probably formed within the seismically imaged melt lens. If this is the case, then we might expect further melt lenses to exist beneath the topographic highs on segments E8 and E9. The absence of highly fractionated magmas on E9, despite the existence of a pronounced axial high (Bruguier & Livermore, 2001), suggests that sea-floor topography is not always a reliable indicator of the presence of a persistent magma chamber.

CHEMICAL VARIATIONS AND CHARACTERIZATION OF COMPONENTS ALONG THE RIDGE

Chemical variations along the ridge

There are systematic variations in composition of lavas along the East Scotia Ridge. Na_8 values, which indicate degree of mantle partial melting (Klein & Langmuir, 1987), are roughly positively correlated with axial depth along the ridge, in that the highest Na_8 samples are generally from deeper parts of the ridge (Fig. 7a), and shallow segments E2 and E8 have low Na_8 values. Most samples from the central segments E4–E7 have relatively high and roughly constant Na_8. Segment E9 also has high Na_8, although it is as shallow as segment E2. The relationships between segments E2–E8 indicate that axial morphology may have been grossly controlled by degree of partial melting. Nb/Yb, a ratio unaffected by additions from the subducting slab, but sensitive to the degree of partial melting, is approximately positively correlated with axial depth (Fig. 7b). Lavas with generally low, N-MORB-like, Nb/Yb ratios dominate in rift-like segments E5–E7 near the centre of the ridge, whereas high Nb/Yb lavas occur in the shallow, inflated segments E2 and E9. However, high Nb/Yb samples have also erupted in segment E4, which is rift-like and deep, but not in

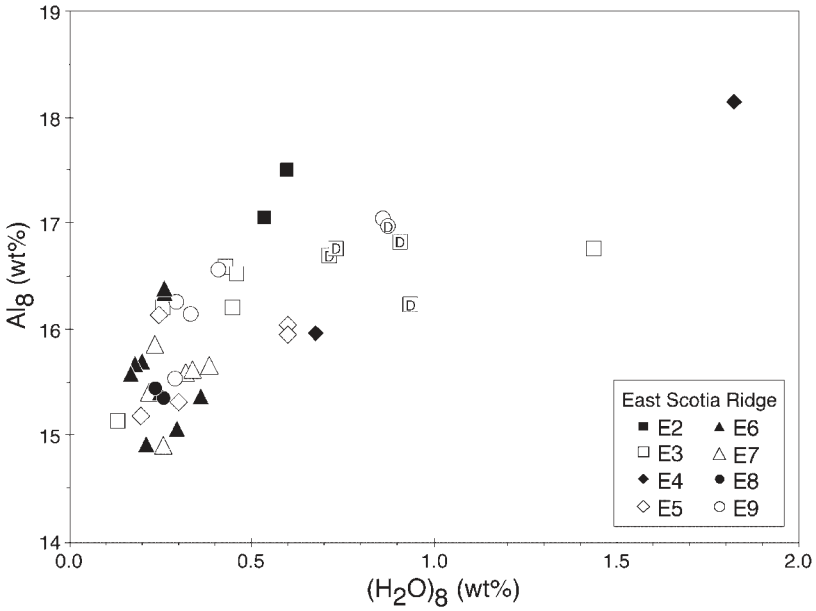

Fig. 6. Fractionation corrected Al_8 (wt %) concentration vs $(H_2O)_8$ (wt %) content for the East Scotia Ridge glasses. The Al_2O_3 content of the magma has been recalculated to 8 wt % MgO along the fractionation vector for each segment in a manner similar to Fe_8 or Na_8 of Klein & Langmuir (1987). Quantified fractionation assemblages (see fractional crystallization calculation in text and in Fig. 4a) and the Rayleigh distillation equation (see, e.g. Cox *et al.*, 1979) have been used to work out the effects of fractionation on magmatic water contents assuming complete incompatibility of water in the cumulate assemblage. Data for dredged samples from segments E3 (D20) and E9 (D23) (see Fig. 2) are from Muenow *et al.* (1980) and are indicated with a 'D'.

segment E8, which is shallow. The high Nb/Yb ratios in segment E2 are not the result of low degrees of partial melting of MORB-source mantle, because low degrees of partial melting would be characterized by both high Nb/Yb and high Na_8. This is not observed (Fig. 7). Because Nb is not likely to have been introduced from the subducting slab (Pearce & Peate, 1995), segments E2, E9 and part of E4 seem to have been supplied by a more enriched, higher Nb/Yb mantle source than MORB. The southern part of segment E8 contains low Na_8 lavas that also have Nb/Yb ratios significantly below the N-MORB ratio. These characteristics are consistent with relatively high degrees of melting of a MORB or sub-arc depleted mantle source.

Variations in REE along the ridge are shown in Fig. 8. Light REE (LREE) abundances can be increased by input from the subducting slab as well as affected by mantle composition and degree of partial melting (Pearce & Peate, 1995). HREE abundances are not affected by additions from the subducting slab. There are significant variations in REE along the East Scotia Ridge. All samples from segments E2 and E9 as well as samples from the overlapping region of segments E3 and E4 (hereafter E3–E4 overlapper) are enriched in LREE. Segments in the central part of the back-arc have low $(La/Sm)_N$ ratios comparable with N-MORB. The along-ridge variations in the $(La/Sm)_N$ ratio closely follow those in Nb/Yb (Figs 7 and 8), consistent with different mantle sources underlying different parts of the ridge. However, variable inputs from the subducting slab may also be present, especially in segments at the ends of the ridge. The $(Dy/Yb)_N$ ratios of samples from the ridge closely follow variations in Na_8, and are lowest in segment E8, where they are similar to N-MORB (Figs 7 and 8). $(Dy/Yb)_N$ ratios are high in segment E9, moderately high in the central segments E5–E7 and relatively low in segment E2. The low $(Dy/Yb)_N$ ratios in segments E2 and E8 indicate that these segments had higher degrees of partial melting than other segments of the ridge, consistent with the low Na_8 values of segments E2 and E8 (Figs 7 and 8).

The positive correlation of $(La/Sm)_N$ with $^{87}Sr/^{86}Sr$ (Fig. 9) reinforces our conclusion that the trace element variations cannot be the result of partial melting alone. The increase in $(La/Sm)_N$ with increasing $^{87}Sr/^{86}Sr$ could be a result either of addition of radiogenic Sr with LREE via subducted sediments, or the presence of an enriched (OIB) mantle component, such as Bouvet mantle plume, under segments E2, E3, E4 and E9. In the following sections, we distinguish the separate mantle and slab-derived components in the back-arc source.

Characterization of components contributing to the back-arc magma source

It has been argued that the characteristic enrichments in volcanic arc rocks of most highly incompatible trace

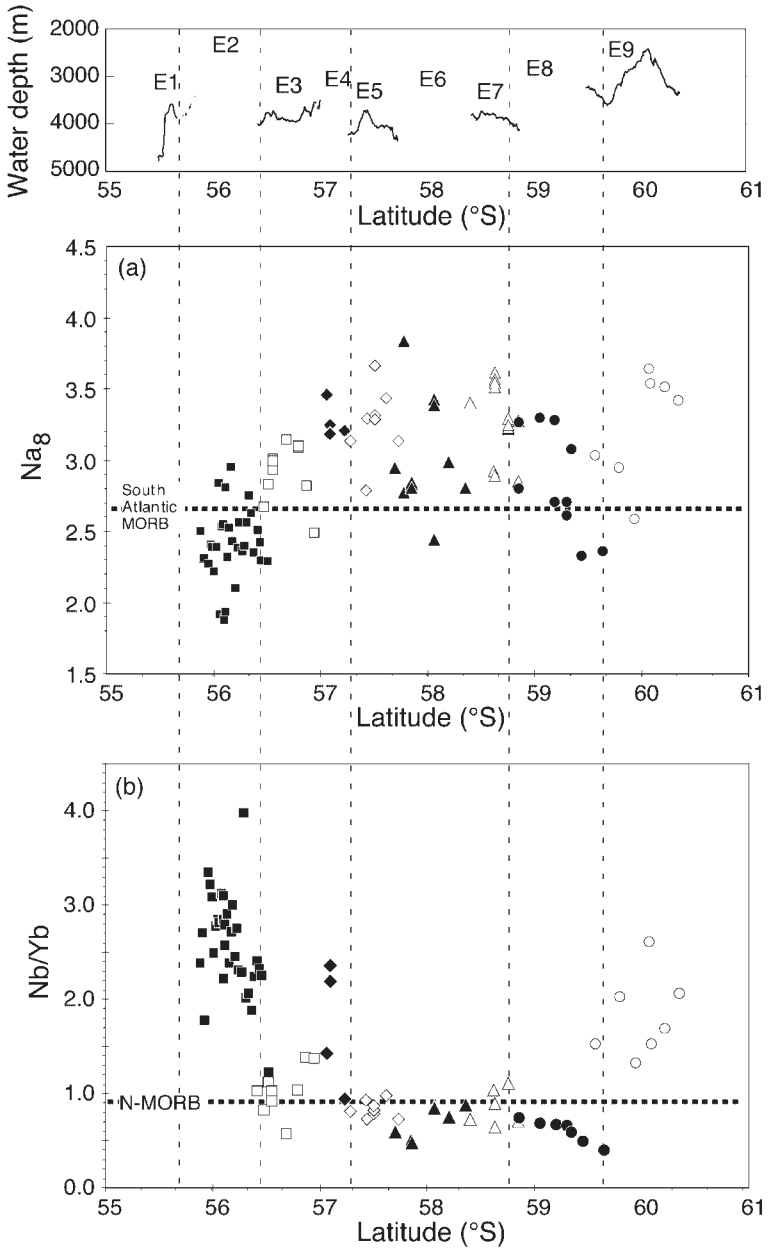

Fig. 7. (a) Na_8 composition [calculated after Klein & Langmuir (1987); see also Fig. 5] and (b) Nb/Yb ratios and water depth as a function of latitude along the East Scotia Ridge. In (a) the dashed line represents the average Na_8 composition of South Atlantic MORB (Klein & Langmuir, 1987) and in (b) the N-MORB average of Hofmann (1988). E2 segment data are, apart from WX42–WX44 (Table 1), from Leat *et al.* (2000).

elements (relative to MORB) result from the contribution of at least two components: sediment or sediment melt and aqueous fluid (Ellam & Hawkesworth, 1988; Ryan *et al.*, 1995; Turner *et al.*, 1996; Elliot *et al.*, 1997; Turner & Hawkesworth, 1997; Class *et al.*, 2000). The sediment component is characterized by high La/Yb, La/Sm and Th/Nb, and is variously regarded as addition of bulk sediment or partial melt of subducted sedimentary rocks. The slab-derived fluid has high B, B/Be, U/Th and Ba/Th, and may consist of variable proportions derived from dehydration of basaltic crust and from dewatering of sediments (Ishikawa & Tera, 1999; Class *et al.*, 2000). Cross-arc geochemical traverses indicate that the fluid component dominates at the volcanic front, where hydration of the mantle causes the greatest amount of melting of the mantle wedge (Ryan *et al.*, 1995). This suggests that subduction components in back-arc spreading centres may be poor in the fluid component.

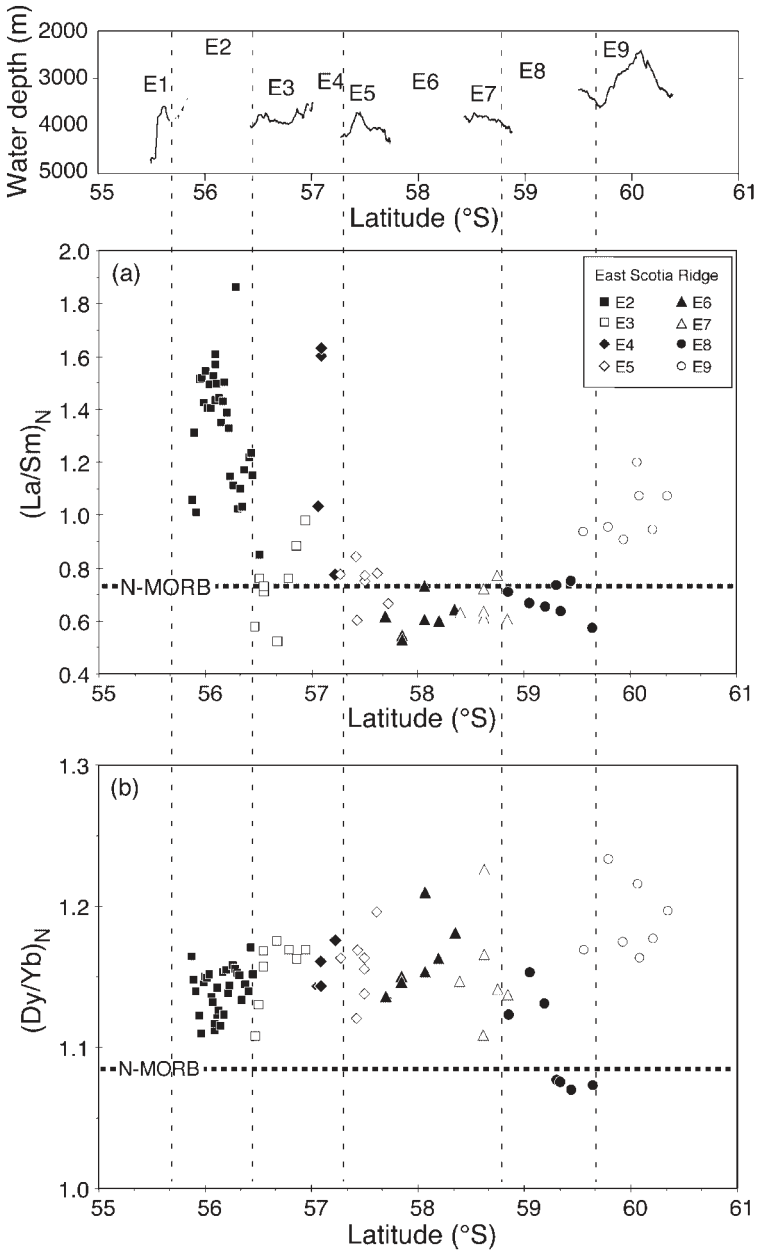

Fig. 8. (a), (b) Chondrite-normalized (Sun & McDonough, 1989) REE ratios and water depth as a function of latitude along the East Scotia Ridge. The vertical lines mark the boundaries of the main ridge segments. In (a) and (b), dashed lines show the N-MORB average of Hofmann (1988). (For E2 segment data, see Fig. 7.)

The addition of subduction components to a mantle source can be assessed by comparing abundances of trace elements in lavas to a reference composition. Pearce & Peate (1995) compared arc lavas with a global MORB array and estimated the percentage contribution from subducted material for various elements. They found that LILE such as Ba, Rb, K, Pb, Th, U and Sr are dominated by subducted material, having a subduction zone contribution of >80%. Class *et al.* (2000) normalized to a local composition to isolate particular components. In Fig. 10, we have compared lavas from segments E2–E9 with sample WX48, which has N-MORB-like values of $(La/Sm)_N$, Nb/Yb, H_2O and $^{87}Sr/^{86}Sr$ (0·58, 0·75, 0·18 wt % and 0·702511, respectively) (Tables 1 and 2). Enrichment factors were calculated by dividing measured element/Yb ratios by the element/Yb ratio of sample WX48, normalized to the Nb/Yb ratio of the sample. This method effectively removes the effects of fractional

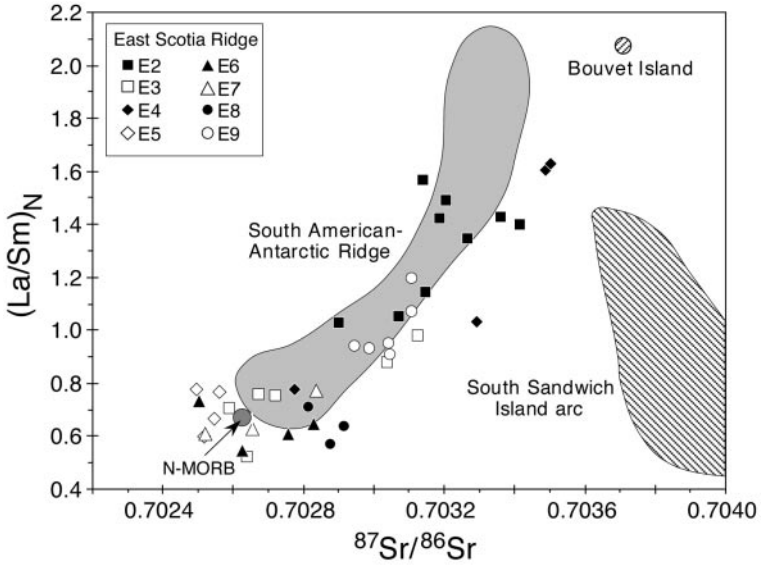

Fig. 9. Variation of $(La/Sm)_N$ vs $^{87}Sr/^{86}Sr$ for lavas from the East Scotia Ridge (E2: Leat *et al.*, 2000), South American–Antarctic Ridge (Dickey *et al.*, 1977; Le Roex *et al.*, 1985), South Sandwich island arc (Pearce *et al.*, 1995), Bouvet Island (Le Roex & Erlank, 1982; Kurz *et al.*, 1998), and the $(La/Sm)_N$ (Hofmann, 1988) and $^{87}Sr/^{86}Sr$ (Ito *et al.*, 1987) composition of N-MORB.

crystallization and different degrees of partial melting for elements of similar incompatibility to Nb. It also removes the effects of different mantle compositions such as plume vs MORB-source mantles. The LILE are ordered in Fig. 10 according to relative importance of the subduction component to their abundances in arcs from Ba (highest) to Sr (lowest) as determined by Pearce & Peate (1995).

Enrichment factors are ≥ 1 in nearly all cases. The enrichment factors of <1 for Sr in some samples probably reflect removal of Sr in plagioclase during fractional crystallization. On the basis of these calculations (Fig. 10), the central part of the East Scotia Ridge (segments E5–E7) shows only a minor influence of a subduction component. Samples from segment E7 consistently have the lowest enrichment factors, below two in most cases. Samples from segments E2–E5, E8 and E9 show highly variable subduction enrichment factors varying from one to 10 and even up to 15 in segment E4, and tend to be highest in the segments near the northern and southern ends of the ridge. Samples with high enrichment factors are interpreted to have very large contributions of LILE from subducted material. There are differences in the relative enrichment of LILE between samples within segments and from segment to segment. In general, Ba, Rb and Th are more enriched than K, U, Pb and Sr (Fig. 10). Th is relatively more enriched in the northern segments E2, E3 and E4 than the southern segments E8 and E9, suggesting regional variations in the importance of different processes or slab-derived components.

The relationships of LILE in the back-arc are shown in Fig. 11. Samples from the South Sandwich Islands form a negative correlation between Ba/Th and Th/Nb. This was interpreted by Leat *et al.* (2000) as a result of variations in the relative amounts of two different slab-derived components in the arc. The high Ba/Th component was interpreted to be aqueous fluid, and the high Th/Nb component was suggested to be sediment. Samples from the East Scotia Ridge are scattered between MORB (and plume mantle) and the arc, and trend away from MORB toward both arc components. An implication of Fig. 11 is that the two components present in the arc also influence compositions in the back-arc. Some samples from E2, E4 and E8 plot toward the high Th/Nb components, whereas most of the rest of the samples trend toward the high Ba/Th component. In this plot, it appears that the fluid component is dominant in most back-arc samples. If the identification of the origin of the components is correct, the few high Th/Nb samples contain a significant input from sediment or sediment melt, whereas the majority of samples are dominated by aqueous fluid from the slab.

The behaviour of these two possible components is further assessed in Fig. 12. Both Ba/Th and Th/Nb correlate positively with H_2O abundances. In the case of Ba/Th, this is consistent with transport of Ba in an aqueous fluid. The positive correlation of Th/Nb with H_2O suggests that Th is transported into the mantle source either in an aqueous fluid, or in a hydrous sediment melt. Several workers have argued that Th is transported from the slab in silicate melts (e.g. Elliott *et al.*, 1997; Turner & Hawkesworth, 1997; Class *et al.*, 2000). This is consistent with experimental data indicating that Th is preferentially partitioned into silicate melts but not into aqueous fluids (Brenan *et al.*, 1995; Johnson & Plank,

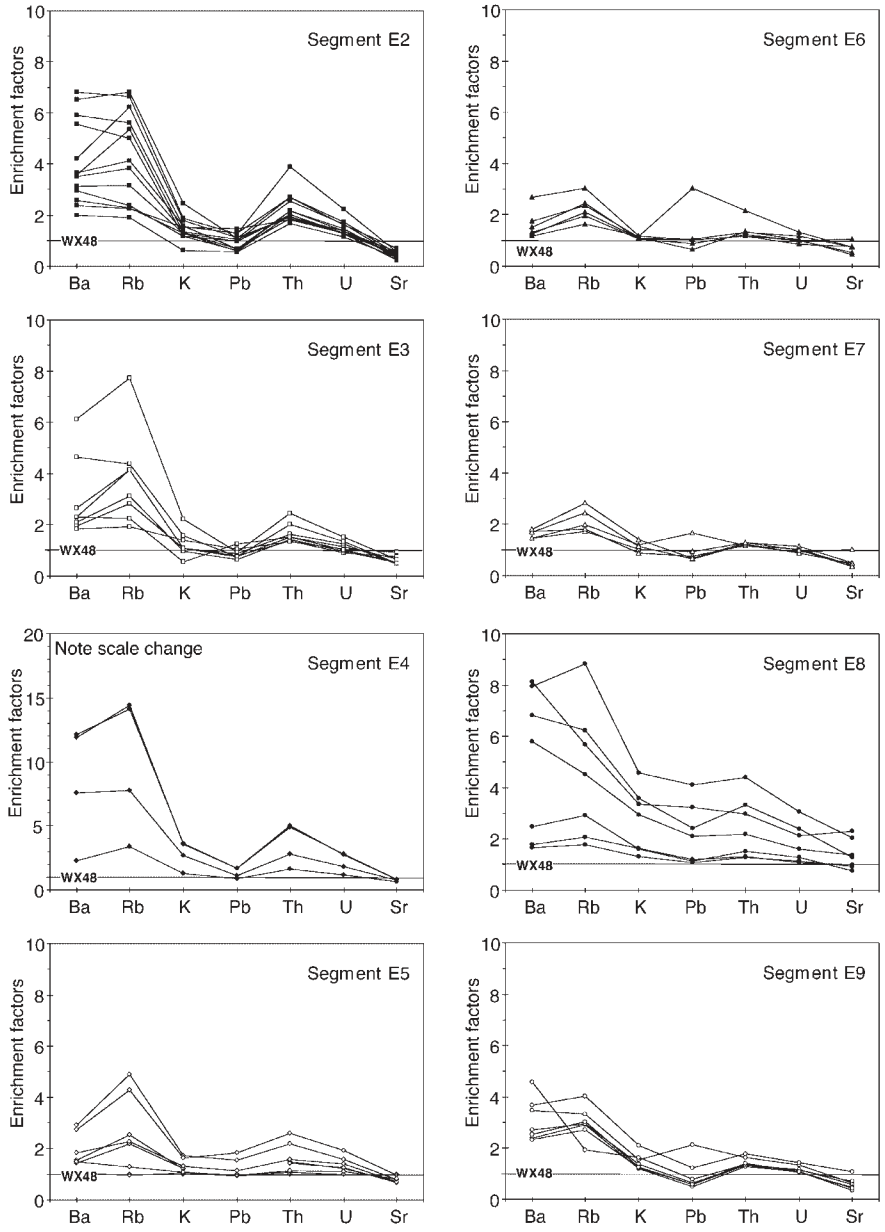

Fig. 10. Estimation of the addition of subduction-related components (Ba, Rb, K, Pb, Th, U, Sr), termed 'enrichment factors', to the East Scotia Ridge magma source relative to a MORB-like 'baseline' sample (WX48) from segment E5. Enrichment factors were calculated by dividing measured element/Yb ratios by the element/Yb ratio of sample WX48 normalized to the Nb/Yb ratio of the sample. This method removes the effects of fractional crystallization, different degrees of partial melting for elements of similar incompatibility to Nb and the effects of different mantle compositions. It should be noted that the scale of the plot showing segment E4 extends to higher values than the other diagrams. (See text for details.)

1999), suggesting that Th requires sediment melting to be efficiently transferred to the arc. However, the partition behaviour of Th in aqueous fluids remains uncertain (Pearce & Peate, 1995) and some workers have suggested that, at high temperature, Th could be transported in an aqueous fluid (Stolper & Newman, 1994).

We have already shown, using Nb/Yb ratios, that there are variations in the composition of the back-arc mantle source independent of subduction components (Fig. 7). In Fig. 13 we investigate the compositional effects of the slab-derived components and plume vs MORB-source mantles on the back-arc lavas. Trends A and B in Fig. 13 diverge strongly from N-MORB. Trend A is characterized by positive correlation of Nb/Yb with Th/Yb, increasing Ta/Nd at constant Th/Nb, and slightly increasing Th/Nd with decreasing $^{143}Nd/^{144}Nd$. This

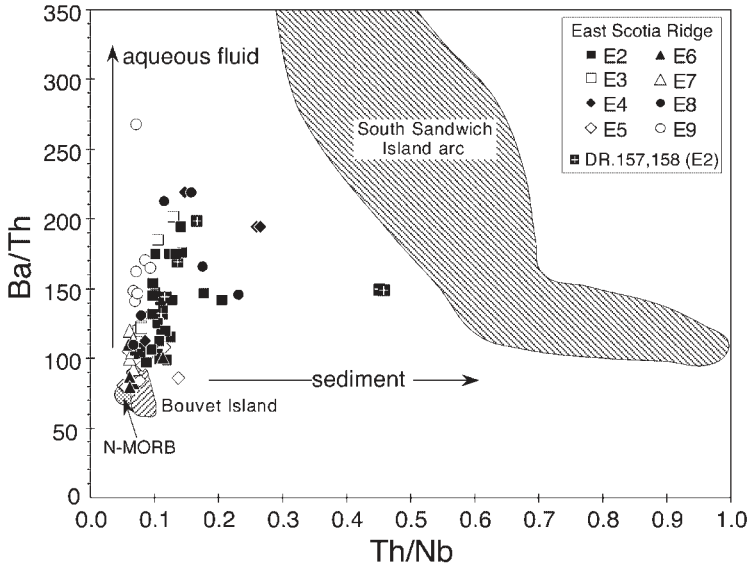

Fig. 11. Variation of Ba/Th vs Th/Nb ratios for lavas from the East Scotia Ridge, South Sandwich island arc (Pearce *et al.*, 1995), Bouvet Island (Le Roex & Erlank, 1982; Weaver *et al.*, 1987), and the composition of N-MORB (Hofmann, 1988). Ba/Th and Th/Nb ratios for samples DR.157 and DR.158 are from D. Harrison (unpublished data, 2000; location sites shown in Fig. 2). The continuous lines with arrows are putative enrichments interpreted to have been caused by aqueous fluid (increasing Ba/Th for constant low Th/Nb ratios) and sediment addition (increasing Th/Nb for constant low Ba/Th ratios) from the subducting slab (see text for details).

trend could be the result of MORB–plume source mixing and/or variable degrees of mantle partial melting. Trend B displays increases in Th/Yb and Th/Nb with moderate increases in Nb/Yb and Ta/Nd, and strong negative correlation between Th/Nd and $^{143}Nd/^{144}Nd$. We interpret this trend to represent MORB–subduction component mixing. Trend A is defined mostly by samples from segments E2 and E9 and therefore occurs symmetrically at the northern and southern ends of the spreading centre. This supports proposals that plume-influenced mantle is migrating into the back-arc around the lateral edges of the subducting plate (Livermore *et al.*, 1997; Leat *et al.*, 2000).

The subduction contribution (Trend B) is seen in the high Th/Yb and Th/Nb of samples from segments E2, E3, E4 and E8. Lavas from the southern part of E8 samples are distinctive in that they have low $(Dy/Yb)_N$ ratios (Fig. 8) and low Nb/Yb and Ta/Nd ratios (Fig. 13). Their mantle source is therefore interpreted to have experienced previous partial melt extraction, and hence depletion in incompatible elements. This is the only place in the spreading centre where previously depleted mantle appears to have been a magma source. Such depleted mantle is also inferred to have formed the source of all the South Sandwich arc lavas (Pearce *et al.*, 1995). Samples from segments E2, E3 and E4 are enriched in the sediment component, trending to high Th/Nb and Th/Nd ratios, at Nb/Yb and Ta/Nd ratios that are higher than MORB. We interpret these compositions to have been formed by addition of the sediment component to an N-MORB-like source mantle. Some samples of segment E2, especially the low-Na_8 group, as well as several lavas dredged on the flanks of the axial high, plot between the two mixing lines (Fig. 13).

The two trends are also clearly seen in plots of U_8 and Nb_8 vs $(H_2O)_8$ (Fig. 14). Trend A shows strong increase in U_8 and Nb_8 with moderate increase in $(H_2O)_8$. This trend is defined by most samples from segment E9 as well as the South American–Antarctic Ridge (note: we have no water contents for the most plume-influenced E2 samples, and so they do not appear in Figs 12 and 14). The South American–Antarctic Ridge is not influenced by the South Sandwich subduction system, but it has been suggested that the ambient MORB-source mantle beneath the ridge has been modified by mantle migrating westward from the Bouvet mantle plume (Le Roex *et al.*, 1985; Kurz *et al.*, 1998). Trend B in Fig. 14 shows constant, MORB-like Nb_8 and increasing U_8 with increasing $(H_2O)_8$ content, implying that magmas of the segments concerned (E2–E5, E9) were produced from sources that experienced addition of water in a subduction component.

To place quantitative constraints on the contribution of the various source components to the different ridge segments, we examined the Sr–Nd–Pb isotope systematics. Figures 15 and 16 show our preferred mixing models between the three end-members involved in the genesis of the East Scotia Ridge lavas: (1) N-MORB-source mantle forming the ambient asthenosphere (Cohen & O'Nions, 1982*b*); (2) OIB-source mantles

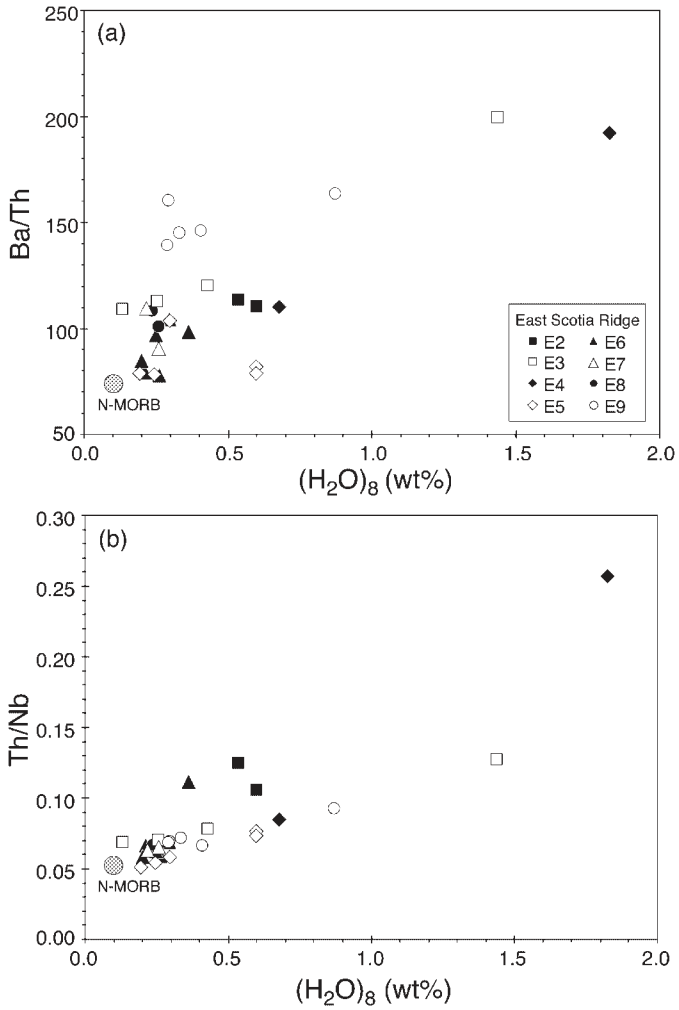

Fig. 12. Variation of (a) Ba/Th and (b) Th/Nb against the $(H_2O)_8$ (wt %) content (see Fig. 6 for calculation procedure) for the East Scotia Ridge glasses.

(McDonough & Sun, 1995) similar to the source of Bouvet Island magmas; (3) sediment components based on South Atlantic bulk sediment (Barreiro, 1983; Ben Othman *et al.*, 1989; Plank & Langmuir, 1998) using two different estimates of the trace element abundances of sediment melt (Class *et al.*, 2000). We also show the composition of the Discovery mantle plume, which is situated at about 44°S, close to the Mid-Atlantic Ridge (Douglass *et al.*, 1999), and which is a similar distance from the East Scotia Ridge to the Bouvet mantle plume.

In Figs 15 and 16, the East Scotia Ridge samples plot close to the MORB end-member and between the MORB end-member and the sediment and mantle plume compositions. This indicates that the MORB component is the most widespread magma source for the East Scotia Ridge, with additional contributions from variable amounts of the sediment and mantle plume components, consistent with interpretations of trace element compositions (Figs 11, 13 and 14). The East Scotia Ridge samples have similar $^{143}Nd/^{144}Nd$ to, but lower $^{87}Sr/^{86}Sr$ than, the South Sandwich island arc. Apart from four samples from the flanks of segment E2, all the East Scotia Ridge samples have lower $^{206}Pb/^{204}Pb$ than the South Sandwich arc. Mixing curves show that the Sr, Nd and Pb isotopic compositions of all the East Scotia Ridge samples (apart from the high $^{206}Pb/^{204}Pb$ samples from segment E2) can be modelled by addition of up to ~2% sediment melt to MORB-source mantle (Figs 15 and 16). Most samples from the central segments E3–E7 can be modelled by addition of <0·4% sediment melt to MORB-source mantle. A group of samples from the flanks of segment E2 shows a clear involvement of a component having $^{206}Pb/^{204}Pb$ ratios of ~19·3, believed to have migrated from the Bouvet mantle plume (Leat

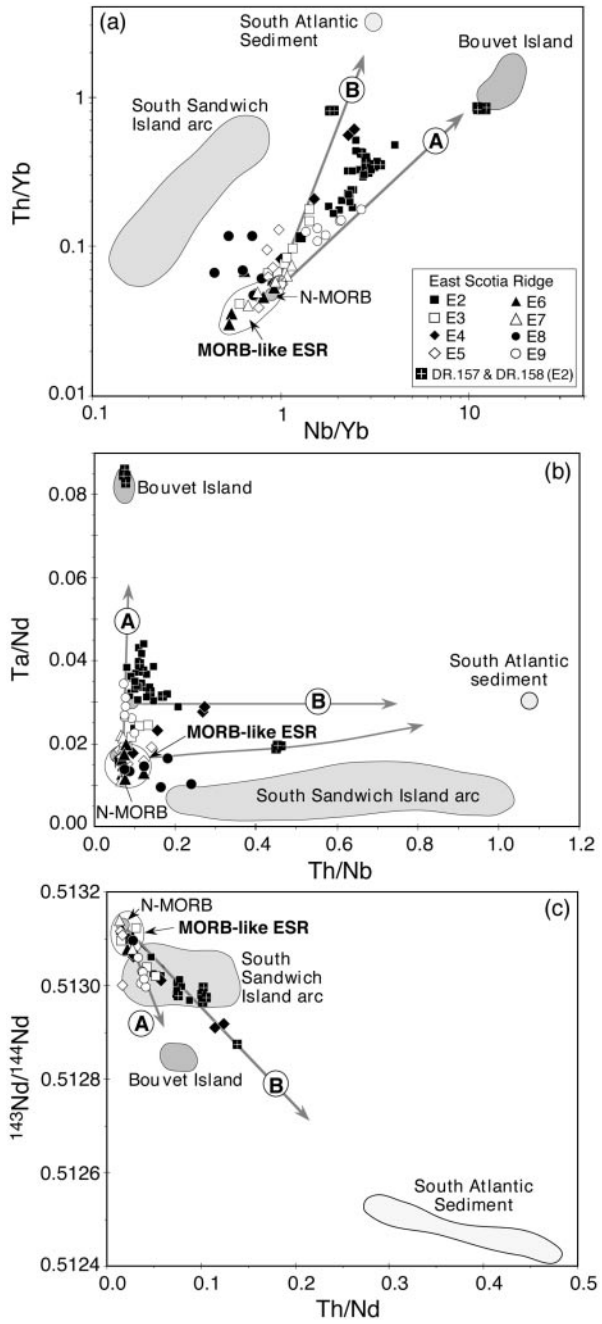

Fig. 13. Variation of Th/Yb vs Nb/Yb (a), Ta/Nd vs Th/Nb (b) and $^{143}Nd/^{144}Nd$ vs Th/Nd (c) for the East Scotia Ridge lavas (E2: Leat *et al.*, 2000), the South Sandwich island arc (Pearce *et al.*, 1995), Bouvet Island (Sun, 1980; Weaver *et al.*, 1987) and bulk South Atlantic sediment (Plank & Langmuir, 1998). For samples DR.157 and DR.158, dredged on the flanks of the E2 segment, data are from D. Harrison (unpublished data, 2000; location sites shown in Fig. 2). Calculated mixing trends (grey lines) between a MORB-like end-member and enriched source components (Bouvet Island: Trend A; bulk South Atlantic sediment: Trend B) are shown. It should be noted that, in (a) and (b), samples from the southern part of segment E8 tend towards the data field of the South Sandwich island arc, which is suggested to be generated from sub-arc mantle modified by subduction-related components from the downgoing slab.

et al., 2000; Pearce *et al.*, 2001). However, it should be noted that it is difficult to distinguish between mixing of sediment and mixing of plume mantle components with a MORB-source mantle using Pb isotope systematics (Fig. 16).

DISTRIBUTION OF MANTLE COMPONENTS

The East Scotia Ridge is tectonically simple, and there are some features of the distribution of magma types within it that appear to be systematic (Fig. 17). The central segments of the ridge are sourced from MORB-source mantle that was influenced only to a minor degree by components from the slab. Departures from MORB-like compositions are strongest close to both northern and southern ends of the ridge. The range in water contents of the magmas, correlating with the range in trace element abundances from MORB-like to arc-like, suggests that decompression melting dominates melt production in the central part of the ridge, and that volatile-fluxed melting is more important at the ends of the ridge.

Segment E2

This segment was discussed by Leat *et al.* (2000), who suggested that the segment tapped both N-MORB and plume mantle sources, and that both aqueous fluid and subducted sediment components had contributed to the range of compositions. The mantle plume component is interpreted to have a high $^{206}Pb/^{204}Pb$ ratio, similar to Bouvet, as such compositions have been identified in a dredge from one flank of the central topographic high that dominates the segment. The segment contains some of the most evolved compositions from the East Scotia Ridge, as a result of extensive fractional crystallization, which is believed to have occurred in a seismically imaged magma chamber (Livermore *et al.*, 1997).

Segment E3

Most samples from this segment are close to N-MORB in composition, but there is a range in compositions to high LILE and low $^{143}Nd/^{144}Nd$. The range in Nd isotopes may be modelled by addition of up to ~0·7% sediment (Fig. 15). Lavas located at the southern end of this segment (E3–E4 overlapper) have high $(H_2O)_8$ contents, up to 1·6%. The segment is interpreted to have erupted magmas derived from an N-MORB source mantle that has been moderately enriched by a water-rich, LILE-bearing subduction component.

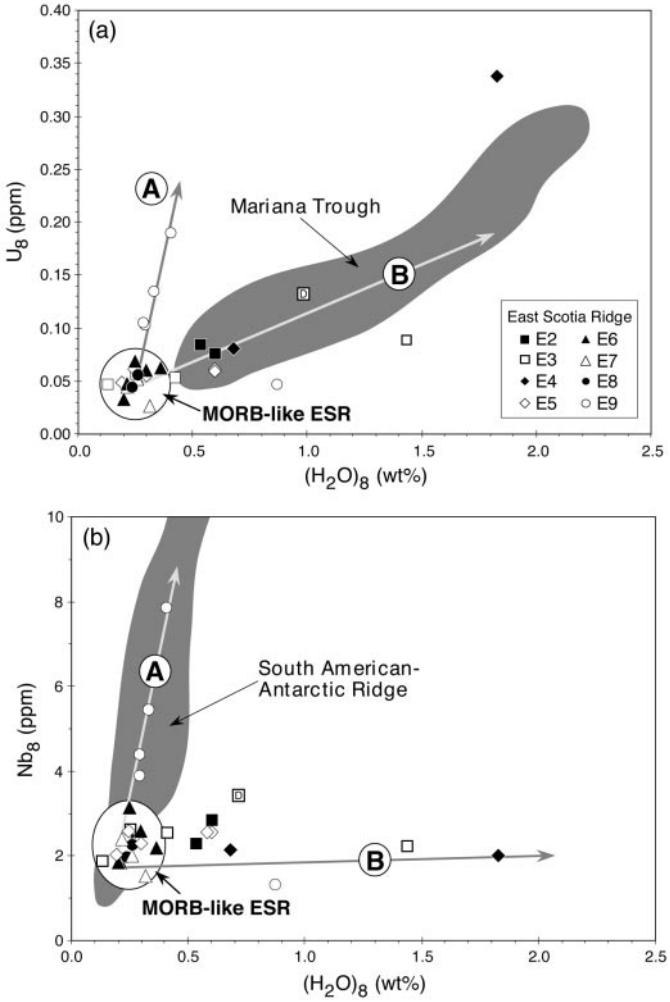

Fig. 14. Variation of U_8 (a) and Nb_8 (b) vs $(H_2O)_8$ (wt %) content (see Fig. 6 for calculation procedure) for the East Scotia Ridge (ESR) volcanic glasses compared with (a) Mariana Trough lavas (Volpe *et al.*, 1987; Stolper & Newman, 1994) and (b) South American–Antarctic Ridge lavas (Le Roex *et al.*, 1985; Michael, 1995). It should be noted that two clear trends can be distinguished in both diagrams. Trend A is observed in segment E9 and South American–Antarctic Ridge lavas showing an increase of U_8 and Nb_8 at nearly constant water contents, whereas Trend B (samples from segments E2–E5) shows in (a) a positive correlation of H_2O with U_8 and in (b) constant Nb_8 with increasing water content. Samples having MORB-like geochemical character are indicated. Water contents for dredged samples from segment E3 (D20; indicated with a 'D') are from Muenow *et al.* (1980); U ppm from Cohen & O'Nions (1982*a*) and Nb ppm from Saunders & Tarney (1979) and are recalculated to 8 wt % MgO (see Fig. 6 for calculation procedure).

Segment E4

Segment E4 is compositionally diverse. Some samples are close to unmodified N-MORB, whereas lavas from the E3–E4 overlapper have very high LILE enrichments, especially Ba and Rb (Fig. 10). The latter have high Th/Yb, $^{87}Sr/^{86}Sr$ and $^{206}Pb/^{204}Pb$ ratios, highest water contents and low $^{143}Nd/^{144}Nd$ relative to all other East Scotia Ridge samples (Figs 6, 13 and 15). Sr–Nd–Pb isotope mixing calculations suggest that the samples can be modelled by addition of 2% sediment melt to a MORB-source mantle (Figs 15 and 16). These relatively extreme compositions are interpreted to have been generated by addition of a very water-rich subduction component that also transported Sr, Th, Nd, Pb, Ba and Rb. The extremely high water content of the samples makes it unlikely that all the water could have been transported by a sediment melt phase, which suggests either that two subduction components were involved (aqueous fluid and sediment melt; see section 'Characterization of components contributing to the back-arc magma source') or that an aqueous fluid transported these elements.

Segments E5–E7

Lavas from the central part of the East Scotia Ridge are close to N-MORB with respect to trace element ratios such as Nb/Yb, $(La/Sm)_N$, Th/Nb and Th/Yb. The

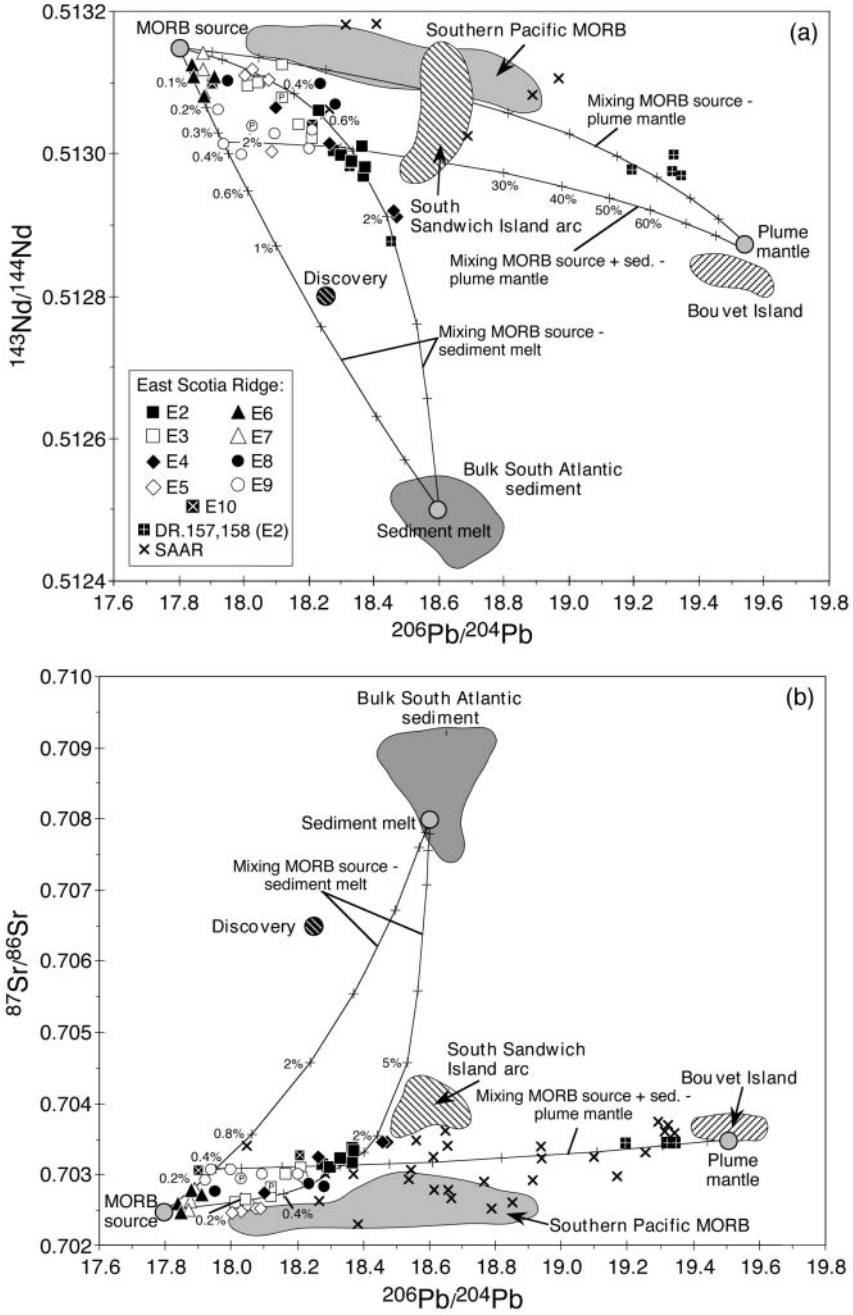

Fig. 15. $^{143}Nd/^{144}Nd$ (a) and $^{87}Sr/^{86}Sr$ (b) vs $^{206}Pb/^{204}Pb$ for the East Scotia Ridge lavas (E2: Leat *et al.*, 2000), South Sandwich island arc (Pearce *et al.*, 1995), South American–Antarctic Ridge (SAAR; Dickey *et al.*, 1977; Le Roex *et al.*, 1985; Ito *et al.*, 1987; Kurz *et al.*, 1998), southern Pacific MORB (Castillo *et al.*, 1998), bulk South Atlantic sediment (Ben Othman *et al.*, 1989; Plank & Langmuir, 1998), Bouvet Island (Sun, 1980; Weaver *et al.*, 1987), and Discovery [average composition from Douglass *et al.* (1999)]. For samples DR.157 and DR.158, dredged on the flanks of the E2 segment, data are from D. Harrison (unpublished data, 2000; location sites shown in Fig. 2). Data from additional E3 (D20) and E9 (D23) samples, indicated with a 'P', are from Pearce *et al.* (2001). Three end-members are suggested to be involved in the petrogenesis of the East Scotia Ridge lavas and calculated mixing trends are indicated. Literature data: 'MORB source' from McKenzie & O'Nions (1995) and Cohen & O'Nions (1982*b*); 'plume mantle' from Sun & McDonough (1989), McDonough & Sun (1995) and McKenzie & O'Nions (1995); 'sediment melt' from Ben Othman *et al.* (1989), Plank & Langmuir (1998) and Class *et al.* (2000). Data used for mixing calculations in (a) MORB source–bulk sediment: $^{206}Pb/^{204}Pb$: 17·8 and 18·6; 0·05, 10 and 3 ppm; $^{143}Nd/^{144}Nd$: 0·5132 and 0·5125; 1·2, 34 and 90 ppm; MORB source–plume mantle: $^{206}Pb/^{204}Pb$: 17·8 and 19·5; 0·05 and 0·15 ppm; $^{143}Nd/^{144}Nd$: 0·5132 and 0·5129; 1·2 and 1·25 ppm; MORB source + 0·4% bulk sediment–plume mantle: $^{206}Pb/^{204}Pb$: 17·94 and 19·5; 0·06 and 0·15 ppm; $^{143}Nd/^{144}Nd$: 0·5130 and 0·5129; 1·23 and 1·25 ppm; in (b) MORB source–bulk sediment: $^{206}Pb/^{204}Pb$: 17·8 and 18·6; 0·05 and 10·3 ppm; $^{87}Sr/^{86}Sr$: 0·7025 and 0·7080; 14·7, 170 and 440 ppm; MORB source + 0·4% bulk sediment–plume mantle: $^{206}Pb/^{204}Pb$: 17·94 and 19·5; 0·05 and 0·15 ppm; $^{87}Sr/^{86}Sr$: 0·7030 and 0·7035; 14·7 and 19·9 ppm.

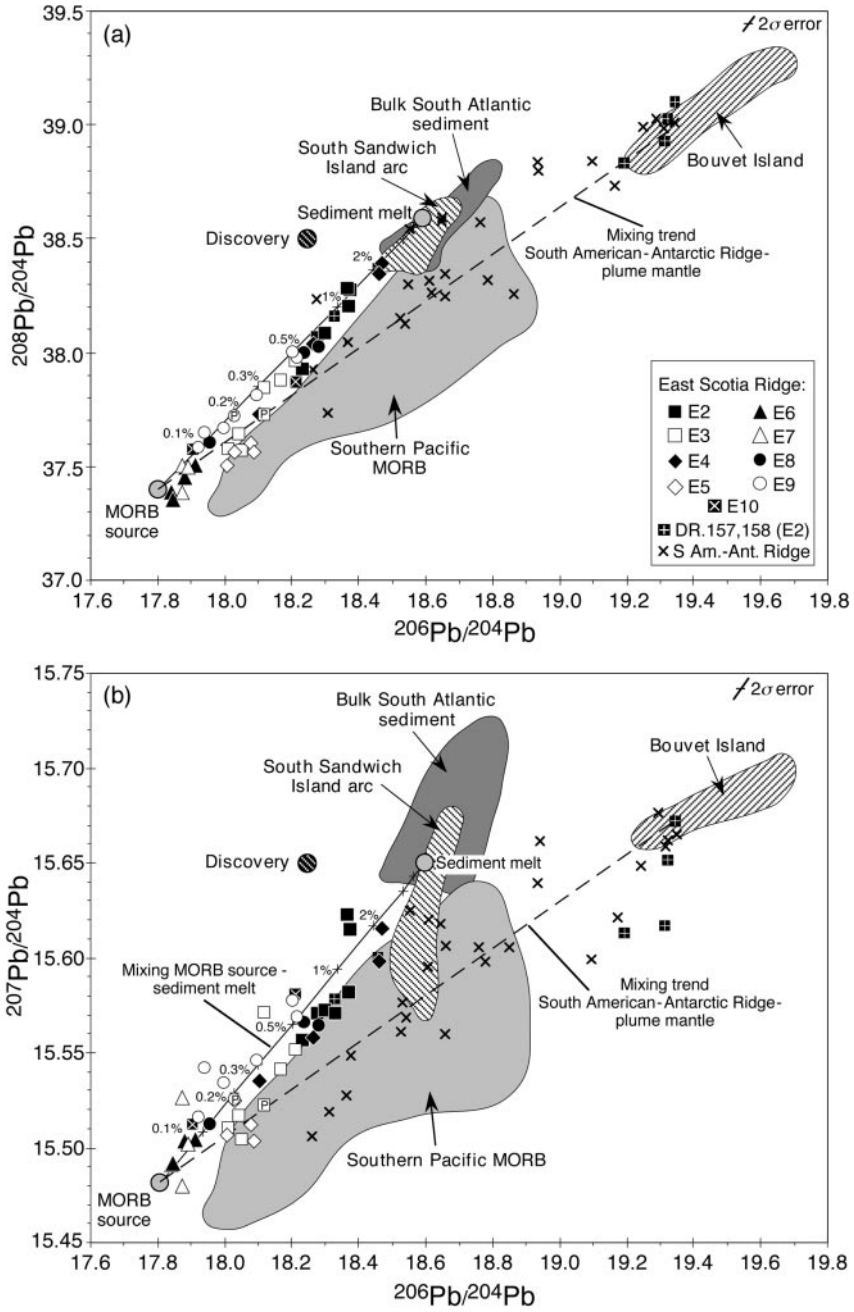

Fig. 16. $^{208}Pb/^{204}Pb$ (a) and $^{207}Pb/^{204}Pb$ (b) vs $^{206}Pb/^{204}Pb$ for the East Scotia Ridge lavas (E2; Leat *et al.*, 2000), South Sandwich island arc (Pearce *et al.*, 1995), South American–Antarctic Ridge (Dickey *et al.*, 1977; Le Roex *et al.*, 1985; Ito *et al.*, 1987; Kurz *et al.*, 1998), Pacific MORB (Castillo *et al.*, 1998), bulk South Atlantic sediment (Barreiro, 1983; Ben Othman *et al.*, 1989; Plank & Langmuir, 1998), and Bouvet Island (Sun, 1980; Kurz *et al.*, 1998), and Discovery (average composition from Douglass *et al.*, 1999). For samples DR.157 and DR.158, dredged on the flanks of the E2 segment, data are from D. Harrison (unpublished data, 2000; location sites shown in Fig. 2). Data from additional E3 (D20) and E9 (D23) samples, indicated with a 'P', are from Pearce *et al.* (2001). Data used for mixing calculations in (a) MORB source–bulk sediment: $^{206}Pb/^{204}Pb$: 17·8 and 18·6; 0·05 and 10 ppm; $^{208}Pb/^{204}Pb$: 37·4 and 38·6 ppm; in (b) $^{207}Pb/^{204}Pb$: 15·45 and 15·62 ppm.

water content and the Rb and Ba concentrations are slightly higher than those of N-MORB. Furthermore, the samples show the highest Na_8 contents compared with the other segments and relatively high $(Dy/Yb)_N$ ratios. On the basis of the slightly elevated water contents and higher Ba/Th ratios compared with N-MORB, we

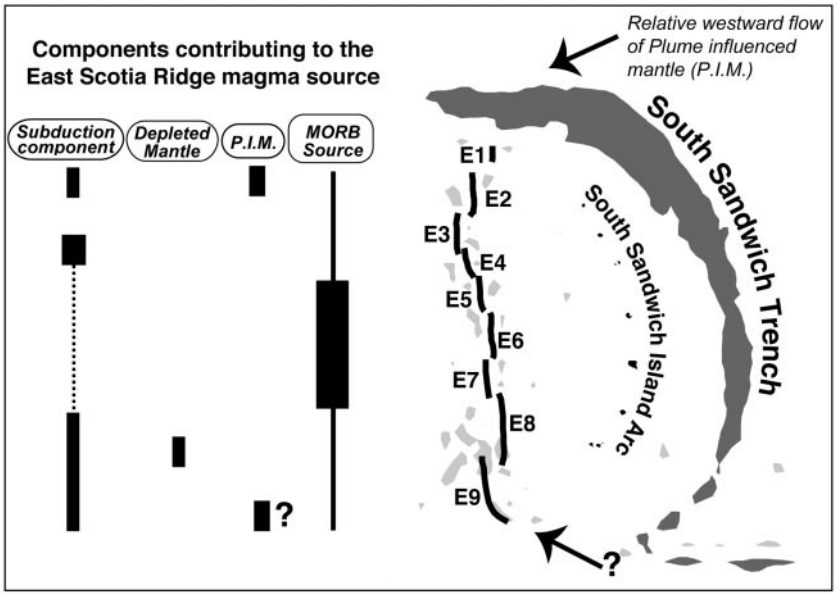

Fig. 17. Sketch of the South Sandwich subdution zone showing the distribution of components contributing to the source of individual back-arc segments. (See text for details.)

suggest that there is a minor influence of a subduction component, probably an aqueous fluid, on an N-MORB mantle source in the central part of the ridge.

Segment E8

Lavas from the southern part of segment E8 are distinctive in having an apparently depleted, low Nb/Yb and $(Dy/Yb)_N$ source, and strong enrichments in LILE (Figs 7b, 8b and 10). The samples are similar to those of the South Sandwich island arc in many trace element ratios (Fig. 13). Their low Nb/Yb and $(Dy/Yb)_N$ ratios indicate that their mantle source was depleted relative to MORB owing to the extraction of a previous melt fraction. Although, in general, mantle has already been processed through the back-arc melting and then is depleted beneath arcs we see a clear involvement of such depleted mantle in the magma source of the lavas erupted in the southern part of segment E8 (Figs 8 and 13), which might be explained by high degrees of melting of a MORB source. The high Ba/Th ratios of the samples, evident in Figs 11 and 12, indicate that segment E8 was affected mainly by aqueous fluid rather than sediment from the subduction zone.

Segment E9

Segment E9 lavas are variable in composition, with progressive north–south trends (Figs 7 and 8). Samples from the southern part of the segment are characterized by high Na_8, high Nb/Yb and $(La/Sm)_N$ ratios, and high Nb_8 and U_8 abundances relative to the northern part (Figs 7 and 14). The relatively high magma production and hence positive topography of this segment suggests a high degree of mantle partial melting. This may be related to plume mantle migrating around the southern end of the slab, or a relatively large influence of subducted water in the source (Bruguier & Livermore, 2001). However, segment E9 lavas have relatively high Na_8 values, implying small degrees of mantle partial melting. They are also relatively poor in geochemical components derived from the subducting slab. The chemical similarity of E9 lavas with lavas from the South American–Antarctic Ridge suggests similar mantle sources, but radiogenic isotopes indicate that the component that sourced segment E9 was unlikely to have been the uncontaminated HIMU Bouvet component.

CONCLUSIONS

(1) Sampling of segments E2–E9 of the East Scotia Ridge has shown that there are striking variations in sources of magmas erupted along the ridge. Some of these variations appear to be related to position within the back-arc basin, and tectonic relationship to the subducting slab.

(2) Segments E2 and E8, both near the ends of the ridge, erupt significantly more evolved magmas than the others. The most evolved magmas are the products of ~50% fractional crystallization for the most mafic observed compositions. The evolved lavas were erupted

on topographic highs along the axes of segments E2 and E8, and the fractionation is interpreted to have occurred in shallow magma chambers. In the case of Segment E2, such an axial magma chamber has been seismically imaged (Livermore *et al.*, 1997).

(3) The central segments of the ridge are sourced from MORB-source mantle that was influenced only to a minor degree by components from the subducting slab.

(4) The northern segment E2 is strongly influenced by plume mantle, which is interpreted to be flowing westward into the back-arc around the edge of the subducting slab (Livermore *et al.*, 1997; Leat *et al.*, 2000; Pearce *et al.*, 2001). The mantle plume component is chemically similar to the Bouvet mantle plume, consistent with evidence for westward flow of mantle from Bouvet, which has been traced geochemically along the South American–Antarctic Ridge (Le Roex *et al.*, 1985; Kurz *et al.*, 1998). Evidence for a mantle plume component in segment E9 at the southern end of the East Scotia Ridge is equivocal.

(5) Subduction components derived from the slab are present in relatively large amounts at the ends of the ridge, and in small amounts in the central segments. Contributions from the slab are chemically heterogeneous, and at least two different subduction components appear to be present, identified as sediment or sediment melt and an aqueous fluid.

ACKNOWLEDGEMENTS

We thank C.-D. Garbe-Schönberg and T. Arpe for their extensive help with the ICP-MS analyses, and Kaj Hoernle and Folkmar Hauff for their valuable assistance with the TIMS analyses. Many thanks go to Dietrich Ackermand, Nigel Bruguier, Alex Cunningham, Graham Eagles, Chris German, Helge Möller, Sven Petersen, Teal Riley, Ulrich Schwarz-Schampera and the captains and crews of the *Polarstern* and *James Clark Ross* for able assistance with the sampling at sea. J. Pearce, R. Stern, T. Elliott and M. Wilson are gratefully acknowledged for their extremely thorough and constructive reviews. This work was funded in part by the Deutsche Forschungsgemeinschaft (DFG) and forms part of the British Antarctic Survey's Oceanic Active Margins project.

REFERENCES

Alvarez, W. (1982). Geological evidence for the geographical pattern of mantle return flow and the driving mechanism of plate tectonics. *Journal of Geophysical Research* **87**, 6697–6710.

Baker, P. E. (1968). Comparative volcanology and petrology of the Atlantic islands arcs. *Bulletin Volcanologique* **32**, 189–206.

Baker, P. E. (1990). South Sandwich Islands. In: LeMasurier, W. E. & Thomson, J. W. (eds) *Volcanoes of the Antarctic Plate and Southern Oceans. American Geophysical Union, Antarctic Research Series* **48**, 361–395.

Barker, P. F. (1995). Tectonic framework of the East Scotia Sea. In: Taylor, B. (ed.) *Backarc Basins: Tectonics and Magmatism*. New York: Plenum, pp. 281–314.

Barker, P. F. & Lawver, L. A. (1988). South American–Antarctic plate motion over the past 50 Myr, and the evolution of the South American–Antarctic ridge. *Geophysical Journal* **94**, 377–386.

Barreiro, B. (1983). Lead isotopic compositions of South Sandwich island volcanic rocks and their bearing on magmagenesis in intra-oceanic island arcs. *Geochimica et Cosmochimica Acta* **47**, 817–822.

Ben Othman, D., White, W. M. & Patchett, J. (1989). The geochemistry of marine sediments, island arc magma genesis, and crust–mantle recycling. *Earth and Planetary Science Letters* **94**, 1–21.

Brenan, J. M., Shaw, H. F., Ryerson, F. J. & Phinney, D. L. (1995). Mineral–aqueous fluid partitioning of trace elements at 900°C and 2·0 GPa: constraints on the trace element chemistry of mantle and deep crustal fluids. *Geochimica et Cosmochimica Acta* **59**, 3331–3350.

Brett, C. P. (1977). Seismicity of the South Sandwich Islands region. *Geophysical Journal of the Royal Astronomical Society* **51**, 453–464.

Bruguier, N. J. & Livermore, R. A. (2001). Enhanced magma supply at the southern East Scotia Ridge: evidence for mantle flow around the subducting slab? *Earth and Planetary Science Letters* **191**, 129–144.

Castillo, P. R., Natland, J. H., Niu, Y. & Lonsdale, P. F. (1998). Sr, Nd and Pb isotopic variation along the Pacific–Antarctic risecrest, 53–57°S: implications for the composition and dynamics of the South Pacific upper mantle. *Earth and Planetary Science Letters* **154**, 109–125.

Class, C., Miller, D. M., Goldstein, S. L. & Langmuir, C. H. (2000). Distinguishing melt and fluid subduction components in Umnak volcanics, Aleutian Arc. *G3* **1**, 1999GC000010.

Cohen, R. S. & O'Nions, R. K. (1982*a*). Identification of recycled continental material in the mantle from Sr, Nd and Pb isotope investigations. *Earth and Planetary Science Letters* **61**, 73–84.

Cohen, R. S. & O'Nions, R. K. (1982*b*). The lead, neodymium and strontium isotopic structure of oceanic ridge basalts. *Journal of Petrology* **23**, 299–324.

Cox, K. G., Bell, J. D. & Pankhurst, R. J. (1979). *The Interpretation of Igneous Rocks*. London: George Allen & Unwin, 445 pp.

Dickey, J. S., Frey, A. F., Hart, S. R. & Watson, E. B. (1977). Geochemistry and petrology of the dredged basalts from the Bouvet triple junction, South Atlantic. *Geochimica et Cosmochimica Acta* **41**, 1105–1118.

Dixon, J. E., Stolper, E. & Delaney, J. R. (1988). Infrared spectroscopic measurements of CO_2 and H_2O in Juan de Fuca Ridge basaltic glasses. *Earth and Planetary Science Letters* **90**, 87–104.

Douglass, J., Schilling, J.-G. & Fontignie, D. (1999). Plume–ridge interaction of the Discovery and Shona mantle plume with the southern Mid-Atlantic Ridge (40°–55°S). *Journal of Geophysical Research* **104**, 2941–2962.

Eggler, D. H. & Burnham, C. W. (1973). Crystallization and fractionation trends in the system andesite–H_2O–CO_2–O_2 at pressures to 10 kb. *Geological Society of American Bulletin* **84**, 2517–2532.

Eiler, J. M., Crawford, A., Elliot, T., Farley, K. A., Valley, J. W. & Stolper, E. M. (2000). Oxygen isotope geochemistry of oceanic-arc lavas. *Journal of Petrology* **41**, 229–256.

Ellam, R. M. & Hawkesworth, C. J. (1988). Elemental and isotopic variations in subduction related basalts: evidence for a three component model. *Contributions to Mineralogy and Petrology* **98**, 72–80.

Elliott, T., Plank, T., Zindler, A., White, W. & Bourdon, B. (1997). Element transport from slab to volcanic front at the Mariana arc. *Journal of Geophysical Research* **102**, 14991–15019.

Fryer, P., Taylor, B., Langmuir, C. H. & Hochstaedter, A. G. (1990). Petrology and geochemistry of lavas from the Sumisu and Torishima backarc rifts. *Earth and Planetary Science Letters* **100**, 161–178.

Gaetani, G. A. & Grove, T. L. (1998) The influence of water on melting of mantle peridotite. *Contributions to Mineralogy and Petrology* **131**, 323–346.

Garbe-Schönberg, C.-D. (1993). Simultaneous determination of thirty-seven trace elements in twenty-eight international rock standards by ICP-MS. *Geostandards Newsletter* **17**, 81–97.

Geist, D. J., McBirney, A. R. & Baker, B. H. (1985). GPP, a program package for creating and using geochemical data files. Eugene: University of Oregon.

Govindaraju, K. (1994). Compilation of working values and sample-description for 383 geostandards. *Geostandards Newsletters* **13**, 1–158.

Gribble, R. F., Stern, R. J., Newman, S., Bloomer, S. H. & O'Hearn, T. (1998). Chemical and isotopic composition of lavas from the northern Mariana Trough: implications for magmagenesis in back-arc basins. *Journal of Petrology* **39**, 125–154.

Hawkesworth, C. J., O'Nions, R. K., Pankhurst, R. J., Hamilton, P. J. & Evensen, N. M. (1977). A geochemical study of island-arc and back-arc tholeiites from the Scotia Sea. *Earth and Planetary Science Letters* **36**, 253–262.

Hawkins, J. W. (1976). Petrology and geochemistry of basaltic rocks of the Lau Basin. *Earth and Planetary Science Letters* **28**, 283–298.

Hawkins, J. W. & Melchior, J. T. (1985). Petrology of Mariana Trough and Lau Basin basalts. *Journal of Geophysical Research* **90**, 11431–11468.

Hergt, J. M. & Farley, K. N. (1994). Major element, trace element, and isotope (Pb, Sr, and Nd) variations in Site 834 basalts: implications for the initiation of backarc opening. In: Hawkins; J., Parson, L. & Allan, J. (eds) *Proceedings of the Ocean Drilling Program, Scientific Results, 135*. College Station, TX: Ocean Drilling Program, pp. 471–485.

Hoernle, K. A. & Tilton, G. R. (1991). Sr–Nd–Pb isotope data for Fuerteventura (Canary Islands) basal complex and subaerial volcanics: applications to magma genesis and evolution. *Schweizerische Mineralogische und Petrographische Mitteilungen* **71**, 3–18.

Hofmann, A. W. (1988). Chemical differentiation of the Earth: the relationship between mantle, continental crust, and oceanic crust. *Earth and Planetary Science Letters* **90**, 297–314.

Ishikawa, T. & Tera, F. (1999). Two isotopically distinct fluid components involved in the Mariana arc: evidence from Nb/B ratios and B, Sr, Nd, and Pb isotope systematics. *Geology* **27**, 83–86.

Ito, E., White, W. M. & Göpel, C. (1987). The O, Sr, Nd and Pb isotope geochemistry of MORB. *Chemical Geology* **62**, 157–176.

Jenner, G. A., Longerich, H. P., Jackson, S. E. & Fryer, B. J. (1990). A powerful tool for high-precision trace element analysis in earth sciences: evidence from analysis of selected U.S.G.S. reference samples. *Chemical Geology* **83**, 133–148.

Johnson, M. C. & Plank, T. (1999). Dehydration and melting experiments constrain the fate of subducted sediments. *G3* **1**, 1999GC000014.

Klein, E. M. & Langmuir, C. H. (1987). Global correlation of ocean ridge basalt chemistry with axial depth and crustal thickness. *Journal of Geophysical Research* **92**(B8), 8089–8115.

Kurz, M. D., Le Roex, A. P. & Dick, H. J. B. (1998). Isotope geochemistry of the oceanic mantle near the Bouvet triple junction. *Geochimica et Cosmochimica Acta* **62**, 841–852.

Le Roex, A. & Erlank, A. J. (1982). Quantitative evaluation of fractional crystallization in Bouvet Island lavas. *Journal of Volcanology and Geothermal Research* **13**, 309–338.

Le Roex, A. P., Dick, H. J. B., Reid, A. M., Frey, F. A., Erlank, A. J. & Hart, S. R. (1985). Petrology and geochemistry of basalts from the American–Antarctic Ridge, Southern Ocean: implications for the westward influence of the Bouvet mantle plume. *Contributions to Mineralogy and Petrology* **90**, 367–380.

Leat, P. T., Livermore, R. A., Millar, I. L. & Pearce, J. A. (2000). Magma supply in back-arc spreading centre segment E2, East Scotia Ridge. *Journal of Petrology* **41**, 845–866.

Livermore, R., Larter, R. D., Cunningham, A. D., Vanneste, L., Hunter, R. J. & the JR09 team (1995). Hawaii-MR1 sonar survey of the east Scotia ridge. *BRIDGE Newsletter* **8**, 51–53.

Livermore, R., Cunningham, A. D., Vanneste, L. & Larter, R. (1997). Subduction influence on magma supply at the East Scotia Ridge. *Earth and Planetary Science Letters* **150**, 261–275.

Livermore, R., Bruguier, N., Cunningham, A. D., Domaschk, U., Eagles, G., Fretzdorff, S., German, C., Maldonado, A., Morris, P. & team of JCR39b (1999). JR39b: deep-towed sonar and seismic survey on the East Scotia Ridge. *InterRidge News* **8**, 34–37.

Mattey, D. P., Carr, R. H., Wright, I. P. & Pillinger, C. T. (1984). Carbon isotopes in submarine basalts. *Earth and Planetary Science Letters* **70**, 196–206.

McDonough, W. F. & Sun, S.-S. (1995). The composition of the Earth. *Chemical Geology* **120**, 223–253.

McKenzie, D. & O'Nions, R. K. (1995). The source regions of ocean islands. *Journal of Petrology* **36**, 133–159.

Michael, P. J. (1995). Regionally distinctive sources of depleted MORB: evidence from trace elements and H_2O. *Earth and Planetary Science Letters* **131**, 301–320.

Michael, P. J. & Chase, R. L. (1987). The influence of primary magma composition, H_2O and pressure on mid-ocean ridge basalt differentiation. *Contributions to Mineralogy and Petrology* **96**, 245–263.

Muenow, D. W., Liu, N. W. K., Garcia, M. O. & Saunders, A. D. (1980). Volatiles in submarine volcanic rocks from the spreading axis of the East Scotia Sea back-arc basin. *Earth and Planetary Science Letters* **47**, 272–278.

Newman, S. & Stolper, E. (1996). Volatiles in magmas from the East Scotia Sea, South Atlantic Ocean. *JAG/RAS Meeting on Subduction Zone Structure, Dynamics and Magmatism, London*. London: Joint Association for Geophysics, Geological Society.

Pearce, J. A. & Peate, D. W. (1995). Tectonic implications of the composition of volcanic arc magmas. *Annual Review of Earth and Planetary Science Letters* **23**, 251–285.

Pearce, J. A., Baker, P. E., Harvey, P. K. & Luff, I. W. (1995). Geochemical evidence for subduction fluxes, mantle melting and fractional crystallization beneath the South Sandwich island arc. *Journal of Petrology* **36**, 1073–1109.

Pearce, J. A., Leat, P. T., Barker, P. F. & Millar, I. L. (2001). Geochemical tracing of Pacific-to-Atlantic upper-mantle flow through the Drake Passage. *Nature* **410**, 457–461.

Peate, D. W., Kokfelt, T. F., Hawkesworth, C. J., van Calsteren, P. W., Hergt, J. M. & Pearce, J. A. (2001). U-series isotope data on Lau Basin glasses: the role of subduction-related fluids during melt generation in back-arc basins. *Journal of Petrology* **42**, 1449–1470.

Peccerillo, A. & Taylor, S. R. (1976). Geochemistry of Eocene calc-alkaline volcanic rocks from the Kastamonu area, northern Turkey. *Contributions to Mineralogy and Petrology* **58**, 63–81.

Pelayo, A. M. & Wiens, D. A. (1989). Seismotectonics and relative plate motions in the Scotia Sea region. *Journal of Geophysical Research* **94**(B6), 7293–7320.

Plank, T. & Langmuir, C. H. (1998). The chemical composition of subducting sediment and its consequences for the crust and mantle. *Chemical Geology* **145**, 325–394.

Roeder, P. L. & Emslie, R. F. (1970). Olivine–liquid equilibrium. *Contributions to Mineralogy and Petrology* **29**, 275–289.

Ryan, J. G., Morris, J., Tera, F., Leeman, W. P. & Tsvetkow, A. (1995). Cross-arc geochemical variations in the Kurile Arc as a function of slab depth. *Science* **270**, 625–627.

Saunders, A. D. & Tarney, J. (1979). The geochemistry of basalts from a back-arc spreading centre in the East Scotia Sea. *Geochimica et Cosmochimica Acta* **43**, 555–572.

Saunders, A. D., Tarney, J., Weaver, S. D. & Barker, P. F. (1982). Scotia Sea floor: geochemistry of basalts form the Drake Passage and South Sandwich spreading centers. *Antarctic Geoscience, International Union of Geological Science, Series B* **4**, 213–222.

Saunders, A. D., Norry, M. J. & Tarney, J. (1991). Fluid influence on the trace element compositions of subduction zone magmas. *Philosophical Transactions of the Royal Society of London, Series A* **335**, 377–392.

Schilling, J.-G., Zajac, M., Evans, R., Johnston, T., White, W., Devine, J. D. & Kingsley, R. (1983). Petrologic and geochemical variations along the Mid-Atlantic Ridge from 29°N to 73°N. *American Journal of Science* **283**, 510–586.

Sclater, J. G., Bowin, C. O., Hey, R., Hoskins, H., Pierce, J., Phillips, J. & Tapscott, C. (1976). The Bouvet triple junction. *Journal of Geophysical Research* **81**, 1857–1869.

Sinton, J. M. & Fryer, P. (1987). Mariana Trough lavas from 18°N: implications for the origin of back arc basin basalts. *Journal of Geophysical Research* **92B**, 12782–12802.

Sisson, T. W. & Grove, T. L. (1993). Experimental investigations of the role of H_2O in calc-alkaline differentiation and subduction zone magmatism. *Contributions to Mineralogy and Petrology* **113**, 143–166.

Stern, R. J., Lin, P.-N., Morris, J. D., Jackson, M. C., Fryer, P., Bloomer, S. H. & Ito, E. (1990). Enriched back-arc basin basalts from the northern Mariana Trough: implications for the magmatic evolution of back-arc basins. *Earth and Planetary Science Letters* **100**, 210–225.

Stolper, E. (1982). Water in silicate glasses: an infrared spectroscopic study. *Contributions to Mineralogy and Petrology* **81**, 1–17.

Stolper, E. & Newman, S. (1994). The role of water in the petrogenesis of Mariana trough magmas. *Earth and Planetary Science Letters* **121**, 293–325.

Sun, S.-S. (1980). Lead isotopic study of young volcanic rocks from mid-ocean ridges, ocean islands and island arcs. *Philosophical Transactions of the Royal Society of London* **297**, 409–445.

Sun, S.-S. & McDonough, W. F. (1989). Chemical and isotopic systematics of oceanic basalts: implications for mantle composition and processes. In: Saunders, A. D. & Norry, M. J. (eds) *Magmatism in the Ocean Basins. Geological Society, London, Special Publication* **42**, 313–345.

Tarney, J., Saunders, A. D. & Weaver, S. D. (1977). Geochemistry of volcanic rocks from the island arcs and marginal basins of the Scotia arc region. In: Talwani, M. & Pitman, W. C. (eds) *Maurice Ewing Series, 1: Island Arcs, Deep Sea Trenches, and Back-Arc Basins*. Washington, DC: American Geophysical Union, pp. 367–377.

Tarney, J., Saunders, A. D., Mattey, D. P., Wood, D. A. & Marsh, N. G. (1981). Geochemical aspects of back-arc spreading in the Scotia Sea and western Pacific. *Philosophical Transactions of the Royal Society of London, Series A* **300**, 263–285.

Todt, W., Cliff, R. A., Hanser, A. & Hofmann, A. W. (1996). Evaluation of a ^{202}Pb–^{205}Pb double spike for high precision lead isotope analyses. In: Basu, A. & Hart, S. (eds) *Earth Processes: Reading the Isotopic Code. Geophysical Monograph, American Geophysical Union* **95**, 429–437.

Turner, S. & Hawkesworth, C. (1997). Constraints on flux rates and mantle dynamics beneath island arcs from Tonga–Kermadec lava geochemistry. *Nature* **389**, 568–573.

Turner, S. & Hawkesworth, C. (1998). Using geochemistry to map mantle flow beneath the Lau Basin. *Geology* **26**, 1019–1022.

Turner, S., Hawkesworth, C., van Calsteren, P., Heath, E., Macdonald, R. & Black, S. (1996). U-series isotopes and destructive plate margin magma genesis in the Lesser Antilles. *Earth and Planetary Science Letters* **142**, 191–207.

Ulmer, P. (1989). The dependence of the Fe^{2+}–Mg cation-partitioning between olivine and basaltic liquid on pressure, temperature and composition. *Contributions to Mineralogy and Petrology* **101**, 261–273.

Vanneste, L. E. & Larter, R. D. (2002). Sediment subduction, subduction erosion and strain regime in the northern South Sandwich forearc. *Journal of Geophysical Research* (in press).

Volpe, A. M., Macdougall, J. D. & Hawkins, J. W. (1987). Mariana Trough basalts (MTB): trace element and Sr–Nd isotope evidence for mixing between MORB-like and arc-like melts. *Earth and Planetary Science Letters* **82**, 241–254.

Weaver, B. L., Wood, D. A., Tarney, J. & Joron, J. L. (1987). Geochemistry of ocean island basalts from the South Atlantic: Ascension, Bouvet, St. Helena, Gough and Tristan da Cunha. In: Fitton, J. G. & Upton, B. G. J. (eds) *Alkaline Igneous Rocks. Geological Society, London, Special Publication* **30**, 253–267.

Woodhead, J., Eggins, S. & Gamble, J. (1993). High field strength and transition element systematics in island arc and back-arc basin basalts: evidence for multi-phase melt extraction and a depleted mantle wedge. *Earth and Planetary Science Letters* **114**, 491–504.